p,xn CROSS SECTIONS IN Pb^{206}

A Thesis

Submitted in Partial Fulfilment of the Requirements

for the degree of

Doctor of Philosophy

by

Harvey Milton Skarsgard

Faculty of Graduate Studies and Research

McGill University

August, 1955

TABLE OF CONTENTS

SUMMARY

Absolute (p,xn) cross sections of Pb^{206} have been measured over the energy range 15 to 65 Mev for x = 1, 2, 3, 4, 5, 6 and 7. Thin target and monitor foils were bombarded together by the internal beam of the 100 Mev McGill synchrocyclotron. Monitoring was based on the known (p,pn) cross section for C^{12}. A 28-channel kicksorter, together with a NaI(Tl) crystal counter, was used to determine the yields of the several reaction products. Chemical separations were avoided in this way. Successive cross sections reached a maximum of the order of one barn. The general shape of an individual (p,xn) cross section is well explained by a model which assumes predominantly particle evaporation from a compound nucleus at low proton bombardment energies and a prompt internal cascade process which is increasingly important at higher energies. However, unpredicted by this model, the even-xn cross sections peak relatively higher than the odd-xn curves. This leads to broad fluctuations in the curve for the sum of the (p,xn) cross sections and suggests that σ_c, the capture cross section for the incident proton, fluctuates similarly.

ACKNOWLEDGEMENTS

The research reported in this thesis followed the experiments by Dr. R.E. Bell on (p,xn) cross sections in bismuth and was suggested by him. Much of the apparatus and the basic experimental technique was due to him. The author gratefully acknowledges this and the constant encouragement and invaluable advice received during the course of the work.

The author wishes to thank Prof. J.S. Foster for his active interest in all phases of this research and, in particular, for his encouragement and aid in the construction of the kicksorter without which the measurements would have been much more difficult. Several helpful discussions were had with Dr. J.D. Jackson who had a very active interest in this work. Dr. L. Yaffe of the McGill Chemistry Department kindly performed certain chemical separations and supplied calibration sources of known strengths. Mr. R.H. Mills was always helpful in supplying cyclotron bombardments.

This research was carried out during the tenure of two Studentships awarded by the National Research Council of Canada, which assistance the author gratefully acknowledges.

I. INTRODUCTION

1. Statement of the Problem

This thesis describes the method of measurement and the results obtained for absolute (p,xn) cross sections in Pb^{206}. Cross sections were measured for the reactions (p,n), (p,2n), (p,3n), (p,4n), (p,5n), (p,6n), (p,7n) in the energy range from their thresholds to 65 Mev. Yields for each of several reaction products in the same target were realized by the aid of a 28-channel kicksorter. This instrument measured the intensities of x-rays and of suitably chosen characteristic gamma rays from individual isotopes. Chemical separations were avoided in this way.

While several measurements of isolated (p,xn) and other reaction cross sections have been made for other elements in the energy range studied here, there is a paucity of systematic measurements for the successive reactions which occur as the incident proton energy is increased.

Measurement of successive (p,xn) cross sections provides a test of nuclear models describing these reactions. Out of such tests more complete and definitive models must evolve. In addition, the quantitative adjustment of the theory to fit the experimental results can lead to the determination of new values for important nuclear constants.

For the heavy elements in the energy range in which the Coulomb barrier is very effective, reactions involving neutron emission are much favoured over those involving proton or other charged particle emission. So, at energies in this region, the sum of the (p,xn) cross sections should give, to a fair approximation, the cross section for capture of the incident proton. This information in turn provides a measure of the nuclear radius of the target nucleus,- that is to say, of the constant r_o in the expression $R = r_o A^{1/3}$ for the nuclear radius of an isotope with mass A.

2. Partial Theoretical Description for Known (p,xn) Cross Sections in Heavy Elements

At energies of bombardment below 30 or 40 Mev it is expected that nuclear reactions proceed predominantly through the formation by the incident particle and the target nucleus of a compound nucleus with all the available energy as excitation energy. Subsequently this energy is mainly dissipated by neutron "evaporation", each evaporated particle emerging on the average with a relatively small amount of energy. The theory describing such processes has been treated extensively[1]. It is believed that the formation of the compound nucleus and its subsequent decay are independent in the sense that the mode of disintegration of the compound nucleus depends only on its nuclear properties and not on the particular way in which it was formed. The formation of the compound nucleus comes about through the strong interaction between the bombarding and target nucleons and the consequent sharing of the available energy. A strong interaction is indicated by a short mean free path for the incident particle in nuclear matter. The formation of the compound nucleus has therefore a high probability at low energies such that the mean free path is short compared to the nuclear radius. Particle evaporation is a relatively slow process as it depends on the statistical chance that enough energy is concentrated on one particle.

Heavy compound nuclei thus formed offer a high Coulomb barrier to proton or other charged particle emission and consequently neutron evaporation is greatly favored. In the energy region for which the evaporation process is predominant (below 30 or 40 Mev) it is assumed that the cross section for formation of a compound nucleus by the incident proton is, to a good approximation, equal to the sum of the cross sections for all (p,xn) reactions

which occur. The qualitative features of evaporation (p,xn) cross sections may be illustrated by considering the case where two neutrons may be evaporated.

Fig. 1 shows diagrammatically the decay of the compound nucleus. If E is the excitation energy of the compound nucleus, the maximum kinetic energy with which the first evaporation neutron may emerge is $(\varepsilon_1)_{max} = E - B_1$ (neglecting recoil energy of residual nucleus), where B_1 is its energy of separation. It turns out that the distribution in energy for the first neutron evaporated is approximately Maxwellian. If ε_1 is the energy of the first evaporated neutron, the distribution in energy is approximately

$$I(\varepsilon_1) = \varepsilon_1 e^{-\frac{\varepsilon_1}{T}} \qquad 1.1$$

Here T is a nuclear "temperature" in energy units. It refers to the residual nucleus after emission of the first neutron and is an adjustable parameter in fitting the theory to experiment.

If the first neutron is emitted with energy between zero and $(\varepsilon_1)_{max} - B_2$, the residual nucleus has enough energy to emit another neutron. B_2 is the binding energy of the second neutron. If, however, the first neutron is emitted with energy between $(\varepsilon_1)_{max} - B_2$ and $(\varepsilon_1)_{max}$ there is not enough energy for evaporation of another. The cross sections may accordingly be written

$$\sigma(p,n) = \sigma_c(p) \frac{\int_{(\varepsilon_1)_{max} - B_2}^{(\varepsilon_1)_{max}} I(\varepsilon_1)\, d\varepsilon_1}{\int_0^{(\varepsilon_1)_{max} - B_2} I(\varepsilon_1)\, d\varepsilon_1 + \int_{(\varepsilon_1)_{max} - B_2}^{(\varepsilon_1)_{max}} I(\varepsilon_1)\, d\varepsilon_1} \qquad 1.2$$

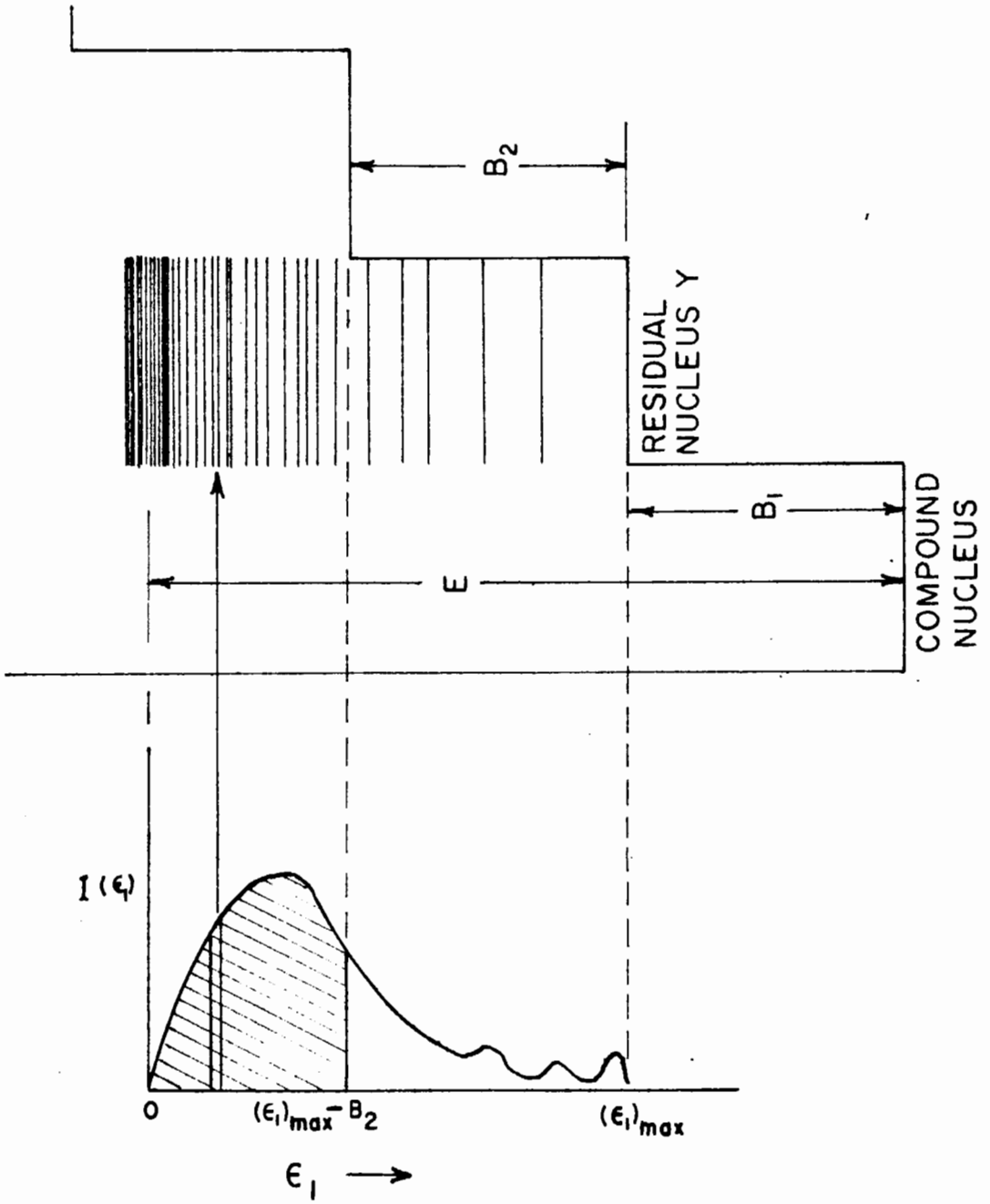

FIG 1. DECAY OF COMPOUND NUCLEUS BY NEUTRON EVAPORATION

$$\sigma(p,2n) = \sigma_c(p) \frac{\int_0^{(\varepsilon_1)_{max}-B_2} I(\varepsilon_1)\, d\varepsilon_1}{\int_0^{(\varepsilon_1)_{max}-B_2} I(\varepsilon_1)\, d\varepsilon_1 + \int_{(\varepsilon_1)_{max}-B_2}^{(\varepsilon_1)_{max}} I(\varepsilon_1)\, d\varepsilon_1} \qquad 1.3$$

These yield, of course, the identity

$$\sigma_c(p) = \sigma(p,n) + \sigma(p,2n) \qquad 1.4$$

The shape of one such (p,xn) cross section is characterized by a peak which rises sharply with increasing proton energy beyond the threshold for the reaction and subsequently falls rapidly due to the onset of the reaction involving evaporation of one more neutron. The absolute magnitude of the cross section peak is closely connected with $\sigma_c(p)$, the cross section for capture of the incident proton to form the compound nucleus. $\sigma_c(p)$ is a strong function of proton energy in the region for which the Coulomb barrier is effective.

Numerical values for $\sigma_c(p)$ have been computed as a function of proton energy for target nuclei of different Z[2],[3]. The calculations, however, are based on a continuum theory of nuclear reactions which averages over individual resonances. It is assumed that the cross section for elastic scattering via the compound nucleus is comparatively small. This limits the applicability of the calculations to energies greater than about 1 Mev. above the threshold for neutron emission. The only information about the nucleus which is used in these calculations is the radius R and K, the wave number of the incident particle wave inside the nuclear surface. Blatt and Weisskopf have neglected that portion of σ_c which gives rise to elastic

scattering while Shapiro has included it. The tabulated values go up to energies of about twice the Coulomb barrier height. For higher energies one must use the effective "geometrical" cross section

$$\sigma_c = \pi (R + \lambda\!\!\!^{-})^2 \left[1 - \frac{B R}{(R + \lambda\!\!\!^{-})\varepsilon}\right] \qquad 1.5$$

where $(R + \lambda\!\!\!^{-})$ is the effective nuclear radius, B is the barrier height and ε is the energy of the relative motion corresponding to wave length $2\pi\lambda\!\!\!^{-}$. At very high energies ($\varepsilon \gg B$) this expression tends toward πR^2. At energies beyond 30 or 40 Mev. this cross section no longer represents the formation of the compound nucleus and neglects the transparency effect.

As noted above, the evaporation theory is expected to describe nuclear reactions below 30 or 40 Mev. At high energies of 100 Mev. or more the mechanism is different and has been described in its general aspects by Serber[4]. The mean free path of the incident particle in nuclear matter is, at these energies, comparable with the nuclear radius and the target nucleus appears somewhat transparent. Indeed, many incident particles pass through the nucleus substantially unaffected. The interaction of the incoming particle with the nucleus is through a succession of quasi-free, two-body collisions with the nucleons, some of which are knocked out with perhaps the incident particle itself emerging with reduced energy. Only rarely is a compound nucleus initially formed. The promptly emitted "cascade" particles may have varying energy and thus leave a residual nucleus with a wide range of excitation energy. The second step of the reaction may then consist of an evaporation of further particles from the excited residual nucleus. In this energy range the cross section for emission of a certain number of particles will vary slowly with energy due to the averaging over the distribution of residual excitations. At any given energy there will be a large number of different reactions competing.

For the energy range between about 30 and 100 Mev there should be a gradual transition from predominantly compound nucleus formation to the internal cascade process.

Calculations have been made by Jackson[5] of cross sections for the expected emission of arbitrary numbers of nucleons, either as prompt or evaporation particles, from heavy nuclei bombarded by neutrons or protons with energies up to 100 Mev. Particular attention has been paid to (p,xn) and (p,pxn) reactions.

The first step in the calculation of the cross section for a specific reaction was the determination of the relative probabilities of the various prompt processes. This information was obtained from Monto Carlo type calculations[5a] based on a succession of quasi-free, two-body collisions. This consists of making numerical calculations for a large number of representative cascades where the states of the interacting collision partners are picked at random out of all possible ones. The answers so obtained can be sorted out into categories corresponding to x prompt neutrons and y prompt protons (denoted as (x,y)) with a distribution of residual excitation energies pertaining to each.

After the emission of the prompt nucleons, the residual nucleus loses energy by the evaporation process; proton evaporation is negligible due to the Coulomb barrier. By assuming a constant nuclear temperature T, Jackson was able to express the probability that exactly x neutrons are evaporated, as a function of the excitation energy of the residual nucleus. (For x = 1, 2 the results agree with those of Weisskopf[1] and they now extend to arbitrary x.)

The cross section for the reaction p,xn could then be obtained by averaging the relative neutron evaporation probabilities over the

excitation distributions for the pertinent prompt processes and weighting with the relative probability for each prompt process. Thus

$$\sigma(p,xn) = \sigma_c(E_o) \sum_j q\ (j,k = 0)\ \langle P(E,\ x-j)\rangle \qquad 1.6$$

where $\sigma_c(E_o)$ is the geometrical cross section seen by the incident proton of energy E_o, $q(j,k)$ is the relative probability for ejection of j prompt neutrons and k prompt protons, and $\langle P(E,x)\rangle$ is the averaged neutron evaporation probability. In these results the nuclear temperature T is a parameter which can be freely adjusted in order to obtain the best agreement with experiment. To a lesser extent the nuclear radius and average neutron separation energy can be adjusted as well.

The calculated (p,xn) cross sections for bismuth are shown in Fig. 2 for x = 1, 2, 3, 4, 5, 6, 7, 8. For these curves $R = 8.9 \times 10^{-13}$ cm ($r_o = 1.5$), B = 7.9 Mev is the average neutron separation energy used, and the nuclear temperature is T = 1.6 Mev. At low energies, the conventional compound nucleus behaviour is evident. As the energy increases the effect of the internal cascade is to give the usual compound nucleus cross section peak a tail extending to higher energies. The magnitude of the tail for successive (p,xn) cross sections becomes higher with increasing x while the magnitude of the peak falls. Correspondingly, the number of contributing cross sections increases with proton energy. (p,pxn) cross sections begin to be important at higher energies. Calculations by Jackson indicate that they are less than .05 barns in the energy region covered by Fig. 2.

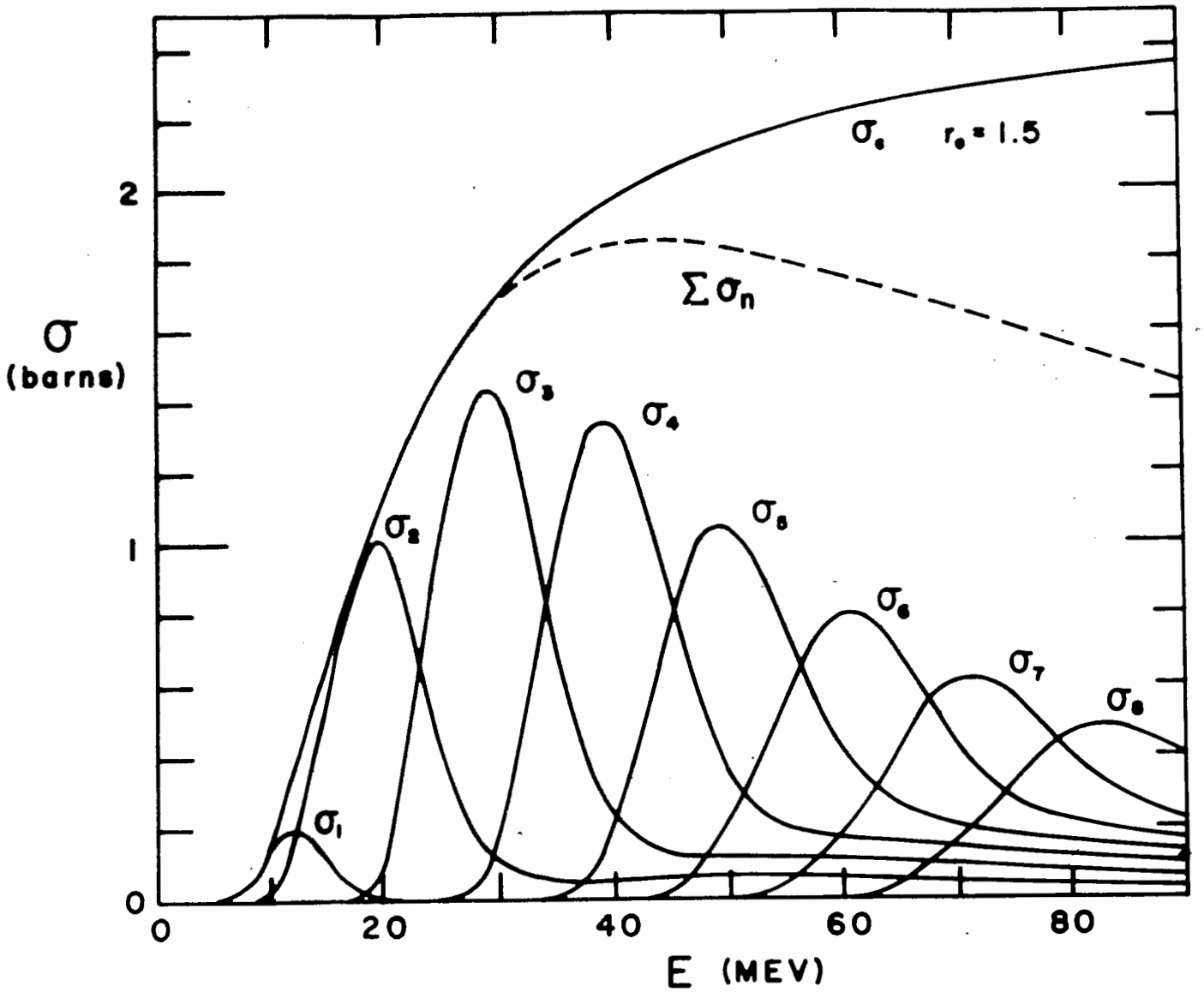

FIG. 2 THEORETICAL (p,xn) CROSS SECTIONS FOR BISMUTH (J.D. Jackson)

3. Previous Experimental Work on (G,xn)* Cross Sections up to 100 Mev.

Bradt and Tendam[6] bombarded stacked foils of silver and rhodium with alpha particles up to 18 mev and observed the yield of radioactive isotopes resulting from (α,n) and (α,2n) reactions. The energy of the alpha particles activating a particular foil in the stack is obtained from the known degradation in energy that the incident alpha particles suffer after passing through a certain amount of matter. The cross sections obtained, as far as they go, show the characteristic compound nucleus shape and can be fitted by evaporation theory by assuming a nuclear temperature T = 1.8 Mev. The sum of the (α,n) and (α,2n) cross sections is equal to the theoretical cross section for formation of the compound nucleus by the impinging alpha particle $\sigma_c(\alpha)$, if a nuclear radius corresponding to $r_o = 1.3 \times 10^{-13}$ cm is used. Bleuler et al[7] later found that more reliable absolute cross section measurements gave, for Ag^{109}, T = 1.7 mev and $r_o = 1.6 \times 10^{-13}$ cm.

Ghoshal[8] has performed an interesting set of experiments which provide a direct proof that the reactions studied proceed through the formation of a compound nucleus. Using a beam of well-defined energy, stacked foils of nickel were bombarded by alpha particles up to 40 mev. Copper foils were bombarded by protons up to 32 mev. Yields of the various radioactive isotopes were determined absolutely by counting positrons emitted in their decay. The reactions studied were as follows:

$Ni^{60}(\alpha,n)\ Zn^{63}$	$Cu^{63}(p,n)Zn^{63}$
$Ni^{60}(\alpha,2n)Zn^{62}$	$Cu^{63}(p,2n)Zn^{62}$
$Ni^{60}(\alpha,pn)Cu^{62}$	$Cu^{63}(p,pn)Cu^{62}$

According to compound nucleus theory each of these reactions proceeds via the formation of the compound nucleus Zn^{64}. Furthermore, the energetics

* G refers to bombarding particle and may be a proton, neutron, alpha particle or deuteron.

of the reactions show that a proton of energy $\mathcal{E}_p$ incident on Cu^{63} and an alpha particle of energy $\mathcal{E}_\alpha = \mathcal{E}_p + 7$ mev incident on Ni^{60} should both form Zn^{64} in the same state of excitation.

Thus, if the decay of the compound nucleus is really independent of the mode of formation, the ratio of cross sections $\sigma(p,n):\sigma(p,2n):\sigma(p,pn)$ for protons of energy $\mathcal{E}_p$ on Cu^{63} should be equal to the ratio of cross sections $\sigma(\alpha,n):\sigma(\alpha,2n):\sigma(\alpha,pn)$ for alpha particles of energy $\mathcal{E}_\alpha = \mathcal{E}_p + 7$ mev incident on Ni^{60}. This is precisely what is observed. (Ghoshal observes cross sections for (,pn) reactions which are higher than those for (,2n). This can be explained qualitatively by considering the level densities in the respective product nuclei Cu^{62} and Zn^{62}. Cu^{62} is odd-odd while Zn^{62} is an even-even nucleus. It is therefore expected that the latter has a much smaller level density and so the number of open channels leading to a 2n decay is small compared to the number open to the pn decay. In this way the effect of the barrier is overcompensated for.)

Meadows[9] has carried out cross section measurements for protons on copper in the region studied by Ghoshal and has extended these and other cross section measurements up to 100 mev. Stacked samples of a single Cu isotope interspaced by aluminum absorbers were bombarded by the internal scattered cyclotron beam with initial energies of 100 and 75 Mev. The energy definition obtained in this way becomes poor for the samples activated by low energy protons. The cross sections for the reactions (p,n), (p,pn), (p,2n) in Cu^{63} show rough agreement with those measured by Ghoshal, but the detailed shapes are somewhat different and absolute values are lower. The (p,n) and (p,2n) cross sections show

roughly the shapes characteristic of evaporation, with the anomaly (observed also by Ghoshal) that the cross section for (p,2n) is small. A small tail persists on the high energy side up to 100 Mev. The p,pn cross section however shows a tail of roughly 20% of the value at the peak. Moreover, the (p,p2n) cross section in Cu^{63} was measured and shows a tailing-off which is about 1/4 of the value at the peak. Cross sections for reactions (p,3n), (p,4n), (p,pn), (p,p3n) and (p,p4n) for protons incident on Cu^{65} were also measured. They each show a peak due to formation by the incident proton of a compound nucleus, and a tailing-off toward higher energies. In qualitative agreement with expectations for an internal cascade process followed by the evaporation of particles from a residual excited nucleus, the magnitude of the cross section in the high energy tail becomes larger in comparison to the value at the peak, as the number of emitted particles in the reaction (prompt and evaporation) increases. An anomalously low peak value for the (p,4n) cross section in Cu^{65} points further to a low level density in the product nucleus Zn^{62}.

Kelly[10] has measured the cross sections for the reactions (α,2n), (α,3n) and (p,2n) in bismuth as well as the shapes of cross sections for the (p,n) and (p,3n) reactions. He bombarded thin films of bismuth evaporated upon thin stacked aluminum foils with a well defined energy beam. Absolute and relative yields were obtained by counting the alpha particle groups emitted in the decay of the product nuclei. The cross sections (α,2n) and (α,3n), measured up to about 40 Mev, show the characteristic rapid rise beyond the thresholds and the expected fall of the first with the onset of the second. The sum of the two cross sections is a smoothly rising curve in close agreement with $\sigma_c(\alpha)$ for r_o between

$1.3 \pm 1.5 \times 10^{-13}$. The cross section for (α,n), though not measured, should be negligibly small over most of the region studied. Of the proton cross sections, only the (p,2n) was measured absolutely. By adopting a half-life in the first case and a branching ratio for the decay of the product nucleus in the second case, σ(p,n) and σ(p,3n) were obtained such that a smooth curve for the sum of all three cross sections gave agreement with a theoretical curve for σ_c(p). Qualitatively, the cross sections appear characteristic of the shapes expected on the compound nucleus theory, with the (p,2n) cross section tailing off on the high energy side, suggesting the beginning of internal cascade effects. The alpha cross sections were not carried to high enough energies to show this. Kelly has also measured cross-sections for deuterons incident on bismuth. The (d,p) and (d,n) cross sections are markedly different from those expected on compound nucleus theory and are accounted for on the basis of a stripping theory in which no compound nucleus is formed. The (d,2n) and (d,3n) cross sections have been summed and compared with the theory for formation of the compound nucleus. While the cross section for (d,2n) depends upon the assumption of a half-life for Po^{209}, the agreement with compound nucleus theory is very poor.

Andre et al[11] have measured cross sections for (p,n), (p,2n) and (p,γ) reactions in bismuth with protons of energies up to about 11 Mev. The stacked foil technique was used and the incident beam was well defined in energy so the results should be more reliable than those of Kelly[9] in this energy region since the latter work must suffer from straggling effects. The (p,n) cross section, based on an assumed half-life as was Kelly's, has not yet reached its peak at 11 mev. The (p,2n)

cross section has been obtained only up to energies less than 1 mev. above its threshold, but is quite different from that of Kelly in this region. This is explainable by straggling effects in Kelly's measurement. Using a nuclear temperature T = 4 Mev and nuclear radius corresponding to $r_o = 1.5 \times 10^{-13}$, the sum of the three cross sections agrees with the theoretical values of Shapiro[3] in the energy region studied.

The first extensive measurements of (p,xn) cross sections have been made by Bell[12] on bismuth. Absolute cross sections for the reactions (p,3n), (p,4n), (p,5n), (p,6n) and (p,7n) were obtained for proton energies ranging from 20 to 85 mev. Bismuth foils ($\sim$80 mg/cm^2) were bombarded with the circulating beam of the McGill synchrocyclotron, together with Teflon foils to serve as flux monitors through the known $C^{12}(p,pn)C^{11}$ cross section. The yields of polonium electron capture product activities of the (p,xn) reactions were determined absolutely by counting the K x-rays. The "window" of a single-channel analyzer was set to include the main peak and escape peak (see Fig. 6a) produced by the x-rays in a NaI(Tl) crystal counter. The results are shown in Fig. 3. Kelly's measurement of the (p,2n) cross section is included; this is modified to represent the cross section which would have been observed with protons having the same spread in energy as the McGill cyclotron beam. As the proton energy is increased, the successive (p,xn) cross sections begin, then rise sharply to a maximum value of the order of one barn. Characteristic of the evaporation process, a particular (p,xn) cross section in the lower energy region, (p,3n) say, rises sharply to its peak and subsequently falls sharply due to the onset of the (p,(x+1)n) reaction, tailing off toward still higher energies to a value which varies only slowly with energy.

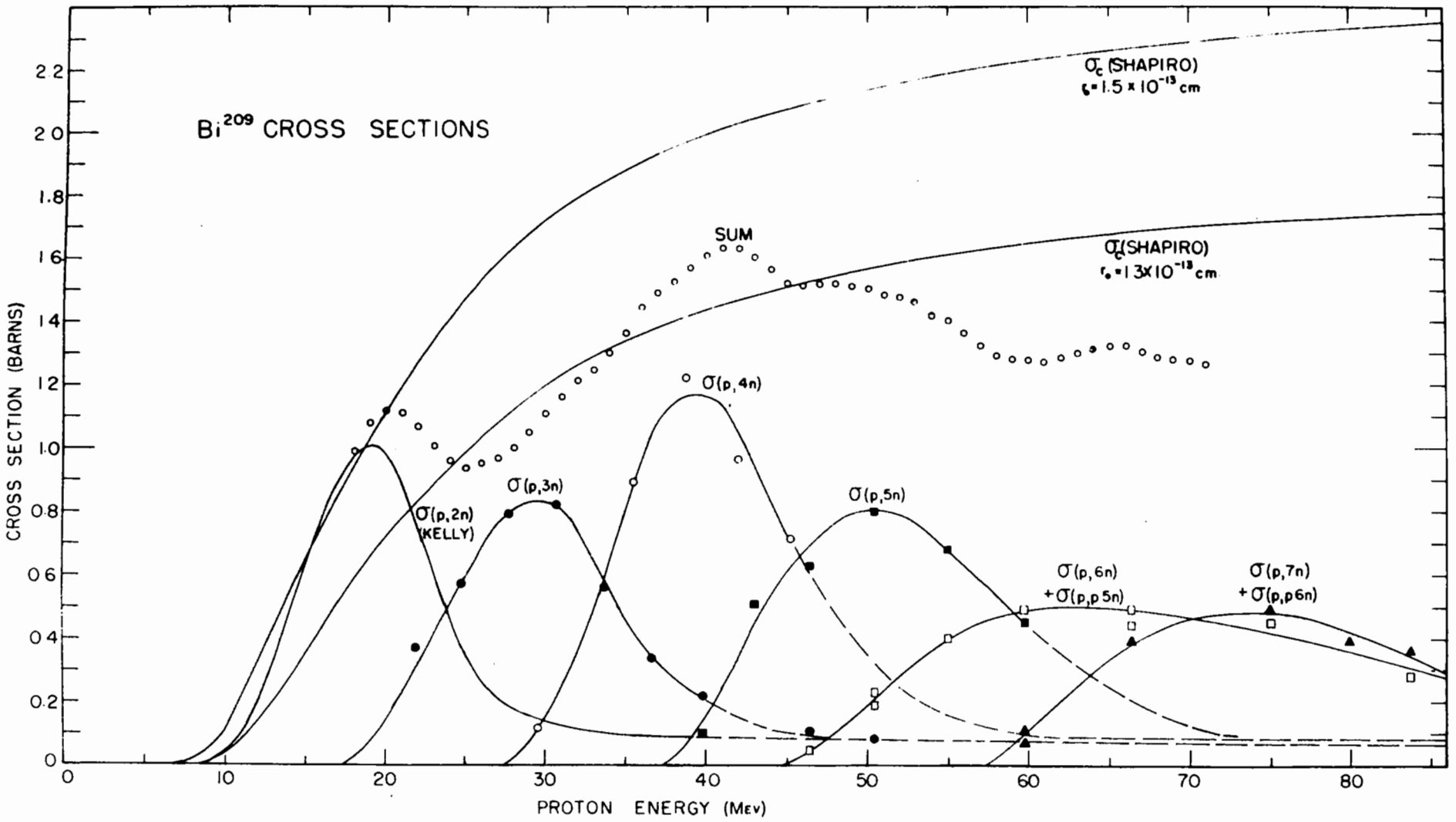

FIG. 3 EXPERIMENTAL CROSS SECTIONS FOR BISMUTH (R.E. Bell)

Toward higher energies and x values the effect of the internal cascade process is increasingly important; the peak is less sharp and the tailing off on the high energy side is more gradual.

The general shape of each individual cross section curve, with the exception of the (p,6n) curve, is well fitted by the theory of Jackson (Fig. 2). However, certain important experimental results are not explained. The (p,2n) and (p,4n) cross sections peak relatively higher than the (p,3n) cross section. This suggests that the evaporation process may favour reactions leading to even-neutron nuclei since the even-xn reactions lead to residual nuclei with an even number of neutrons and the odd-xn reactions lead to nuclei with an odd number of neutrons. An alternative explanation, however, also presents itself. Fig. 3 shows the curve obtained by summing all (p,xn) cross sections occurring at each energy. Up to about 40 mev it follows roughly the theoretical $\sigma_c(p)$ for r_o between 1.3 and 1.5 x 10^{-13} cm. There are, however, broad fluctuations in the sum curve. Main peaks occur at about 18 and 40 mev. If, then, $\sigma_c(p)$ is not a smoothly varying function of energy but has peaks at 20 and 40 mev, the (p,2n) and (p,4n) cross sections would be relatively higher and the (p,3n) cross section relatively lower than predicted by the theory of Jackson. Somewhat similar fluctuations have been observed in the total cross section for low energy neutrons and have been studied according to a model by Feshbach et al[19].

Above about 40 mev, the curve for the sum of the measured (p,xn) cross sections falls progressively lower than $\sigma_c(p)$ for r_o = 1.4 x 10^{-13} cm, say. This is at least partly due to the increasing importance of reactions other than (p,xn), which are not observed. The general shape of the experimental sum curve, averaged over its fluctuations, is in good

qualitative agreement with the shape of the theoretical $\Sigma \sigma n$ curve calculated by Jackson. Jackson's results were calculated using $r_o = 1.5 \times 10^{-13}$ cm and cross sections are on the average higher than the experimental curves.

The experimental measurements for the (p,6n) cross section are made by observing the yield of the daughter activity and so include the (p,p5n) contribution as well. The agreement with the shape of the theoretical sum of the two cross sections is not very good.

Further investigations have been made of (p,xn) and other reactions[13-17] and the feasibility of interpreting them in terms of compound nucleus formation and internal cascade effects has been studied.

II. METHOD AND APPARATUS

1. General Method

The lead target foils irradiated were about 80 mg/cm^2 in thickness. The sample foil was cut to closely the same shape (1/4" in width) as the monitor foil with which it was bombarded and one was placed carefully over the other so that they both "saw" the same incident beam. The foils were backed by sufficient copper to absorb completely the protons which passed through the foils so that multiple traversals were avoided.

Kirkaldy[18] has made a study of the energy distribution of the internal proton beam at various radii. The average of the distribution is estimated from the energy the protons would have at a given field and radius - if the orbit were always centered at the geometrical centre of the magnet - by subtracting an energy increment corresponding to a one inch reduction in radius. This is due to the radial oscillation which causes the beam to circulate as though about a centre which itself performs a rotation about the magnetic field - determined centre point. The half-width (energy width at half maximum) of the incident proton beam at any radius is given as the energy equivalent of a 1.5 inch increment in the radius and the shape of the distribution is asymmetrical and falls off sharply at energies above the peak but more gradually on the low energy side. (1.5 inch is thought to be an upper limit for the energy spread as the methods of measuring it suffer from errors which tend to give too large a spread.)

The effect of the energy distribution on the general shape of a measured (p,xn) cross section is small in as much as the square of the half-width of the former is small compared to the square of the half-width of the cross section curve. In particular, the energy distribution

distorts the cross section near the threshold, giving a threshold which is too low, and reduces the value at the peak of a cross section.

At reduced beam current (to prevent overheating of the foils) irradiation times of from one to five minutes were usually sufficient to activate the samples so that convenient counting rates were obtained. The activities of the target and monitor foils were then examined with a NaI(Tl) scintillation counter delivering pulses to a 28-channel kicksorter.

The monitor reactions in copper and carbon produce positron emitters. The absolute yield of these activities was determined by observing the annihilation radiation following the absorption of the positrons in material placed about the monitor sample. The particular crystal counter used was calibrated (II. 2.) so that the efficiency for counting full energy events was known as a function of the incident gamma ray energy and the distance from the source to the near surface of the crystal.

The activity induced in the target sample was examined with the kicksorter. Usually there were several different reaction products in each active sample. All reaction products decayed by electron capture. Absolute yields of a particular reaction product were based upon the decay curve for the K x-rays following K-capture. This usually necessitated an analysis of the gross K x-ray decay curve in order to determine the separate decay due to each reaction product. In order to determine relative yields and, in some cases, as a check on absolute yields, the intensity of a suitably chosen gamma ray emitted in the decay of a particular reaction product was observed. The relative yields could be converted to absolute yields by normalization to the absolute yield obtained from the K x-rays at some bombardment energy for which

the reaction in question was predominant or at least where the decay of the specific reaction product could be easily distinguished in the gross K x-ray decay curve.

In a sample of uniform thickness of n atoms/cm^2, we have for the total number of active atoms produced through a particular reaction with a cross section σ

$$N = n\, p\, \sigma \qquad 2.1$$

where p is the total number of protons which pass through the sample. If the irradiation time t_r is short in comparison with the mean life of the activity produced, (always true in these experiments) we have for the initial disintegration rate,

$$(\lambda N) = \lambda\, n\, p\, \sigma \qquad 2.2$$

and

$$\lambda N = c\, A_i \qquad 2.3$$

where A_i is the observed initial counting rate for K x-rays of the isotope in question and c is a number which is determined by the following factors (to be discussed in II, 4): the ratio of K-capture to total electron capture, internal conversion of γ-rays emitted in the decay, self-absorption of x-rays by the source, fluorescent yield, and the counter efficiency. If the reaction product decays by other means besides electron capture the branching ratio also enters into the value for c. λ is the disintegration constant.

Equations 2.2 and 2.3 give for the reaction cross section

$$\sigma = \frac{c\, A_i}{\lambda\, n\, p} \qquad 2.4$$

A_i is determined from the decay curve of the particular isotope. n is obtained from a micrometer measurement of the target thickness and the known density of the material. p is given by the activity of the monitor sample through an equation obtained analogous to 2.4.

$$p = \frac{c_M A_{iM}}{\lambda_M n_M \sigma(M)} \quad \text{for } t_r \ll \frac{1}{\lambda_M} \qquad 2.5$$

where c_M is determined by the efficiency for counting annihilation quanta in the full energy peak, and includes a factor of 1/2 which accounts for the fact that there are two annihilation quanta emitted per β^+ decay. The monitor samples of copper and teflon were surrounded by sufficient material to absorb completely the positrons emitted.

A sample calculation of a reaction cross section is given in Appendix I.

2. Proton Beam Monitoring

Proton flux monitoring for the (p,xn) cross section measurements in Pb^{206} was based upon the known $C^{12}(p,pn)C^{11}$ cross section[20]. A teflon ($(CF_2)_n$) foil of 27 mg/cm^2 thickness was irradiated together with a lead foil for each bombardment so that the same proton beam passed through both. Teflon was used since it is relatively heat-resistant. The 20.5 min C^{11} positron activity was converted to annihilation radiation (two .511 mev quanta for each positron annihilated) by completely absorbing the positrons in matter surrounding the teflon. The decay curve tailed off into a 110 min F^{18} activity so that it was necessary to count for about five hours after irradiation.

Aamodt et al[20] have published a cross section curve for the $C^{12}(p,pn)C^{11}$ reaction from its threshold to 340 mev. It was obtained in three steps. Up to 32 mev the cross section was measured by Aamodt et al using the stacked foil and absorber method with a proton beam from a linear accelerator. Above 100 mev they used a cyclotron-accelerated external proton beam of 340 mev degraded to various energies by means

of copper absorbers of appropriate thicknesses. In the region from 32 to 100 mev, the excitation curve obtained by Hintz[20a] was fitted in absolute magnitude to the measurements at lower and higher energies. Hintz employed the stacked foil technique and a cyclotron-accelerated proton beam of 110 mev. Only recently, Crandall et al[20b] have re-measured the carbon cross section from 170 to 350 mev. They find a somewhat different shape from that of Aamodt et al and attribute this to the poor absorber geometry used by Aamodt et al. In addition, near 350 mev where poor absorber geometry does not affect the measured cross section of .41 mb obtained by Aamodt et al, Crandall et al obtain a cross section of 36 mb. This difference is attributed to the improved techniques for beta counting used by Crandall et al. They therefore suggest that the cross section determined by them from 170 to 350 mev be joined to the curve from 18 to 100 mev which is obtained from the data of Aamodt et al upon normalization by a factor of 36/41. Therefore, for the (p,xn) cross section work on Pb^{206} and on bismuth, monitoring is based upon the $C^{12}(p,pn)C^{11}$ cross section curve which is obtained by multiplying the cross section of Aamodt et al by a factor of 36/41.

For energies below about 25 mev the monitoring was achieved through use of the known $Cu^{63}(p,n)Zn^{63}$ and $Cu^{63}(p,pn)Cu^{62}$ cross sections[8]. Copper foils of 36 mg/cm^2 were irradiated together with the lead targets, and the annihilation radiation resulting from absorption of the positron activity was counted. Zn^{63} decays 93% by positron emission and 7% by electron capture; Cu^{62} decays 100% by positron emission. By comparison of the proton beam monitoring indicated by the carbon activity with that by the (p,pn) reaction in copper, over the energy range from 25 to 30 mev,

it was concluded that the published copper cross section relative to carbon was about 39% too high. Ghoshal's values were therefore normalized in absolute magnitude to the carbon cross section by multiplying them by 1/1.39. Meadows[9] has measured the absolute cross sections for $Cu^{63}(p,n)Zn^{63}$ and $Cu^{63}(p,pn)Cu^{62}$ and he finds values which are roughly 30% lower than Ghoshal's. The shapesof Meadow's cross sections differ appreciably from Ghoshal's, due at least in part to a poorer energy resolution in his incident proton beam.

In order to apply the monitor cross sections to the proton beam of the McGill synchrocyclotron, account was taken of its energy spread. The "effective" or "smeared" cross section was calculated from the measured curves by assuming a square distribution in energy with a width at any energy equivalent to a 1.5 inch increment in the radius at that energy. Fig. 4 shows the "smeared" carbon and copper cross sections. Ghoshal's copper cross sections have, in addition, been multiplied by a factor of 1/1.39. The smearing affects the curves only slightly; the thresholds are lowered and the peak values of the relatively narrow copper cross sections are reduced somewhat.

In the energy range from about 15 to 20 mev over which the (p,n) and (p,pn) cross sections in copper are both of appreciable magnitude, the effective energy of the McGill proton beam can be measured. This is accomplished by finding the energy at which the ratio of cross sections for the two reactions is equal to that indicated by the respective yields obtained in a certain bombardment. Since in the energy region from 15 to 20 mev, the (p,n) cross section is falling fairly rapidly while the (p,pn) cross section is rising sharply, the method is quite sensitive. At 20

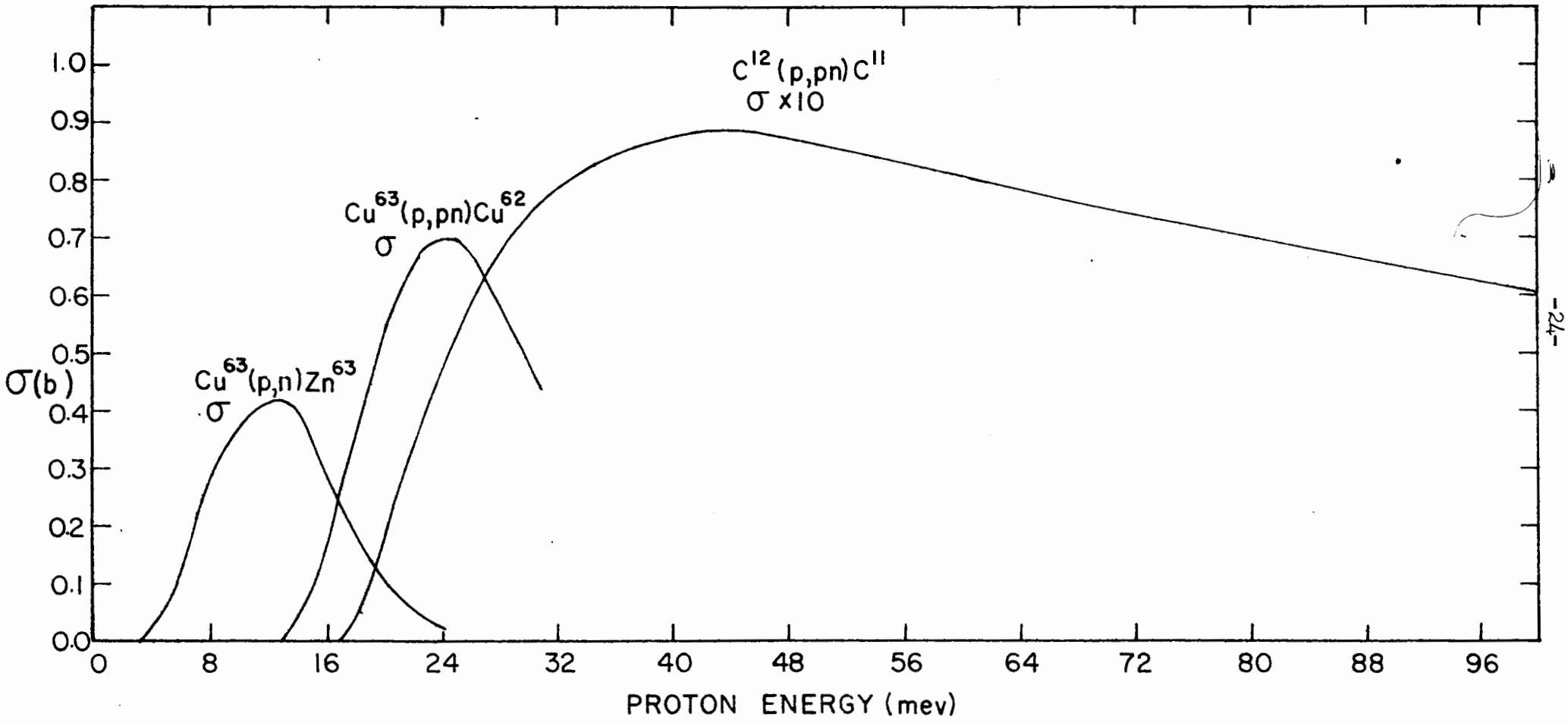

FIG 4. MONITOR REACTION CROSS SECTIONS

mev, the measured effective energy was 1.4 mev higher than that deduced from the magnetic field. This was important in comparing the carbon and copper cross sections as, in the region where they can be compared, they are both strong functions of the energy.

Considerable effort was put into attempting to monitor by integrating the proton beam current (absorbed by the copper block) after it has passed through the foils, practically undiminished. An integrator circuit, due to Dr. R.E. Bell, was built for this purpose and is described in Appendix II. However, it was found that there was an appreciable contribution to the current, presumably from low energy ions drifting about in the vacuum, which was a function of radius and which, unfortunately, varied from time to time. The idea was therefore abandoned.

3. Gamma Spectroscopy Apparatus

(a) Schematic description of Experimental Arrangement

Fig. 5 shows the experimental arrangement employed for the examination of sample activities.

An efficiency-calibrated crystal scintillation counter was used which consists of a 1 1/2 in. diameter by 1 in. high crystal of NaI(Tl) mounted on a DuMont 6292 photomultiplier. The anode pulse from the photomultiplier is fed to the input of a cathode-follower which delivers a negative pulse with a typical rise time of 0.5 μsec and a relatively slower tail-off to give a pulse duration of about 3 μsec. Amplification with a reversal of sign is brought about using the second amplifying ring of an Atomic Instruments A1 amplifier[21] and the kicksorter is supplied with positive pulses of up to about 30 volts in height. Upon amplification by the kicksorter amplifier (gain -2.7) and another change

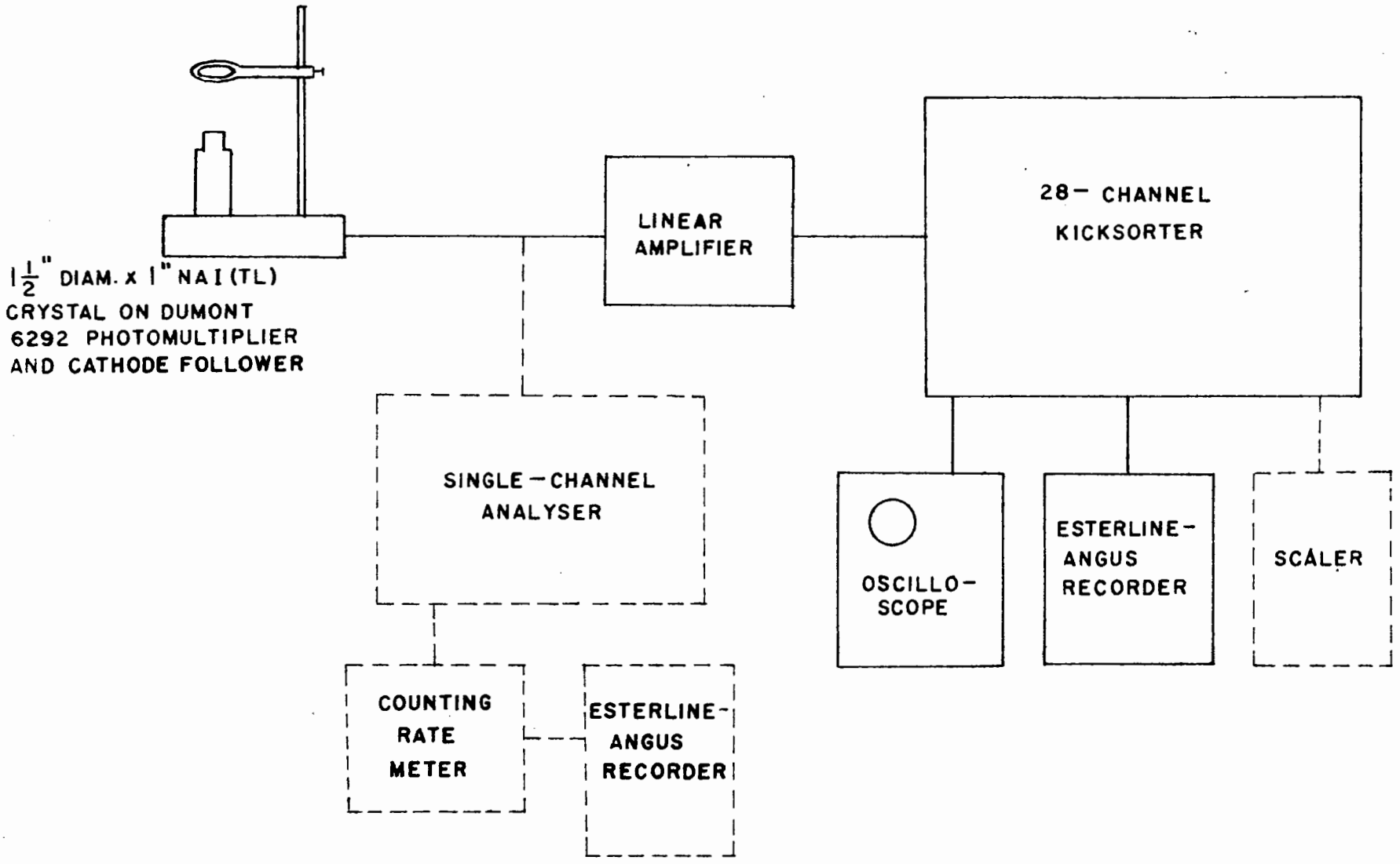

FIG 5. EXPERIMENTAL COUNT-SORTING ARRANGEMENT

of sign, the pulses are sorted out with respect to their height, into 28 channels of equal width. The total accumulated number of pulses in any one channel is represented as a d.c. voltage output and the final or growing spectrum of pulse heights is observed on an oscilloscope through use of a fast rotary switch which samples, successively, the channel outputs and rotates in synchronization with the sweep of the oscilloscope. A slow rotary sampling switch is used in conjunction with an Esterline-Angus graphic ammeter to give a permanent record of the final spectrum which can then be analysed. Provision was also made, in the design of the kicksorter, for counting with a scaler the total number of pulses sorted into any one channel.

The output pulses from the crystal scintillation counter could alternatively be delivered to a single channel pulse height analyser. The design of this instrument is due to Dr. R.E. Bell[22]. With this instrument, the pulse height distribution, upon amplification to a convenient size range, is observed with a single channel which is adjustable with regard to its width and the lowest pulse height admitted into it. The channel "energy" can be adjusted manually or caused to scan automatically, over a period of time, the entire pulse height spectrum. In the latter case the pulses admitted into the channel are conveniently delivered to a counting rate meter, the output of which can be fed to an Esterline-Angus or Speedomax graphic ammeter to give a continuous spectrum of the distribution of pulse heights. Because of the continuously scanning channel of adjustable width, this instrument has a better resolution than the kicksorter and is useful for observing detail in a pulse height spectrum.

Both the 28-channel kicksorter and single-channel analyser are equipped with coincidence circuitry. There is also available a fast coincidence circuit, due to R.E. Bell[23], with an adjustable resolving time as low as about 20×10^{-9} sec. It is, as a result, possible to do a large variety of definitive coincidence gamma spectroscopy experiments which may be indirectly of use in cross section studies or of independent value in providing information on decay schemes.

(b) Use of 28-channel kicksorter in determination of yields

The kicksorter was built at McGill according to a design by Dr. R.E. Bell and its operation has been described in detail in a forthcoming publication[24] and in a report for the McGill Radiation Laboratory[25]. For the purpose of demonstrating its use in the work described for this thesis, it is sufficient to denote the main features and how they are made use of.

Pulses are sorted out with respect to their height into 28 channels and each is stored as an increment of voltage on an integrating condenser. There are two alternative sizes of condenser in each channel so that an integrated voltage output of 100V corresponds respectively to 10^3 or 10^4 counts in that channel. This allows for magnification, by a factor of 10 in height, of any portion of a spectrum observed.

The d.c. outputs of the channels are sampled by a fast rotary switch which sweeps through them successively at 1800 r.p.m. and provides an oscilloscope histogram of the spectrum at any time during its growth, or at the termination of a count. This visual presentation is especially useful when setting up the photomultiplier voltage and amplifier gain most convenient for observing the spectrum of interest. The channel

outputs can also be sampled by a manually operated rotary switch and read off as voltages on a panel voltmeter. In counting a spectrum which peaks in a certain channel it is useful to set the manual switch to read the output of this channel and then count for as long as is required to give full scale reading of 100V. A third rotary switch driven by a slow synchronous motor samples the 28 channel voltages over a period of two minutes and leads to an Esterline-Angus graphic ammeter which records the spectrum as a histogram. This is the permanent record which is later analysed.

The discriminator bias for successive channels can be selected from among three scales. For a certain photomultiplier voltage and linear amplifier gain setting, one of these, the "main" scale, provides kicksorting coverage of a certain pulse height range. The "lower half" and "upper half" scales then can be used to examine the lower and upper halves of the "main" scale spectrum, but with twice the number of channels. The improved resolution helps to show detail in a complicated spectrum.

Methods of gamma ray spectroscopy using scintillation counters have been extensively discussed, for example, in the book of K. Siegbahn[26]. The efficiency for counting gamma rays emitted by a radioactive source is a product of the geometrical (solid angle) efficiency and the absorption probability for the gamma rays in the crystal. For energies below about 1 Mev the important processes by which a gamma ray is absorbed are the photoelectric and Compton effects. In a photoelectric event, (neglecting surface effects), the full energy of the incident gamma ray is delivered up to an electron which is stopped in the crystal and the resulting scintillation produces an electronic pulse corresponding to

the full energy. For a Compton event, the energy of the struck electron is delivered to the crystal but the scattered quantum may or may not escape. If the scattered quantum does not escape, a pulse corresponding to the full energy of the primary gamma ray is produced but pulses for which it does escape produce a continuum with a calculable upper limit in energy (from the mechanics of the Compton process for a backward-scattered gamma ray). The statistical nature of the collection of light at the photocathode and the resultant cascade of electrons in the photomultiplier produces a smearing out of pulse heights. The resolution of a crystal counter is measured as the ratio $\Delta E/E$ of the width at half-maximum of a full energy peak to the energy corresponding to the peak. If non-uniformity effects are negligible, the shape of a peak is Gaussian and the resolution is inversely proportional to the square root of the energy E.

Fig. 6 shows kicksorter pulse height distributions due to the .074 mev lead K x-ray and the .661 mev barium gamma ray; the NaI(Tl) counter specified in Fig. 5 was used. At .074 mev, absorption is almost entirely by the photoelectric process. This results in a full energy peak and, for this energy, also an "escape" peak. The latter is a surface effect due to the fact that the lead x-rays are absorbed in a relatively thin surface layer of the NaI(Tl) crystal so that some of the iodine x-rays following a photoelectric event escape. Such events give rise to an "escape" peak at an energy lower than that of the full energy peak by an amount corresponding to the energy of the iodine x-ray. In Fig. 6(a) the lead x-ray spectrum is superimposed on a background of Compton continuum due to higher energy gamma rays; the resolution is about 23%. The spectrum for

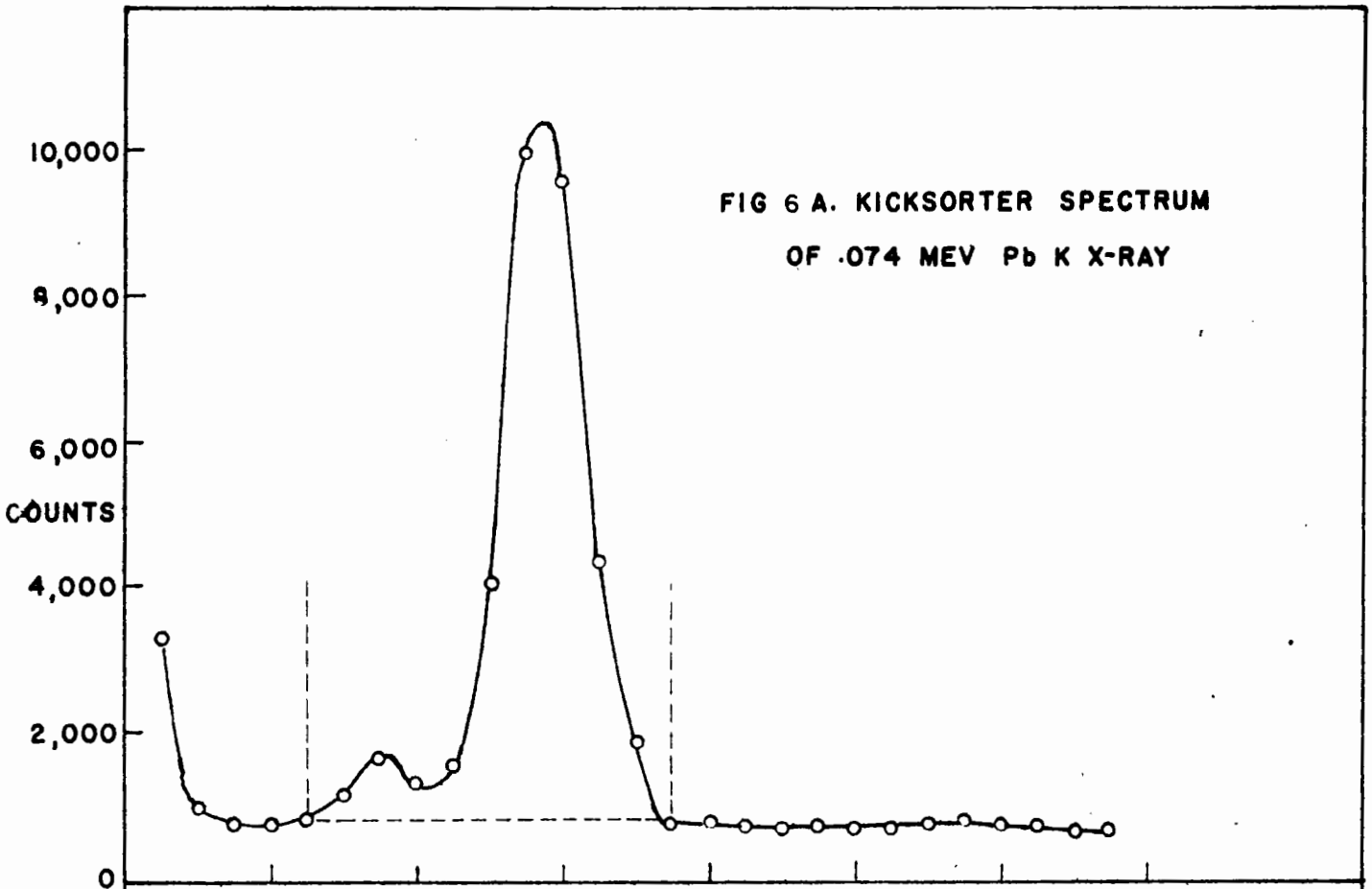

FIG 6 A. KICKSORTER SPECTRUM OF .074 MEV Pb K X-RAY

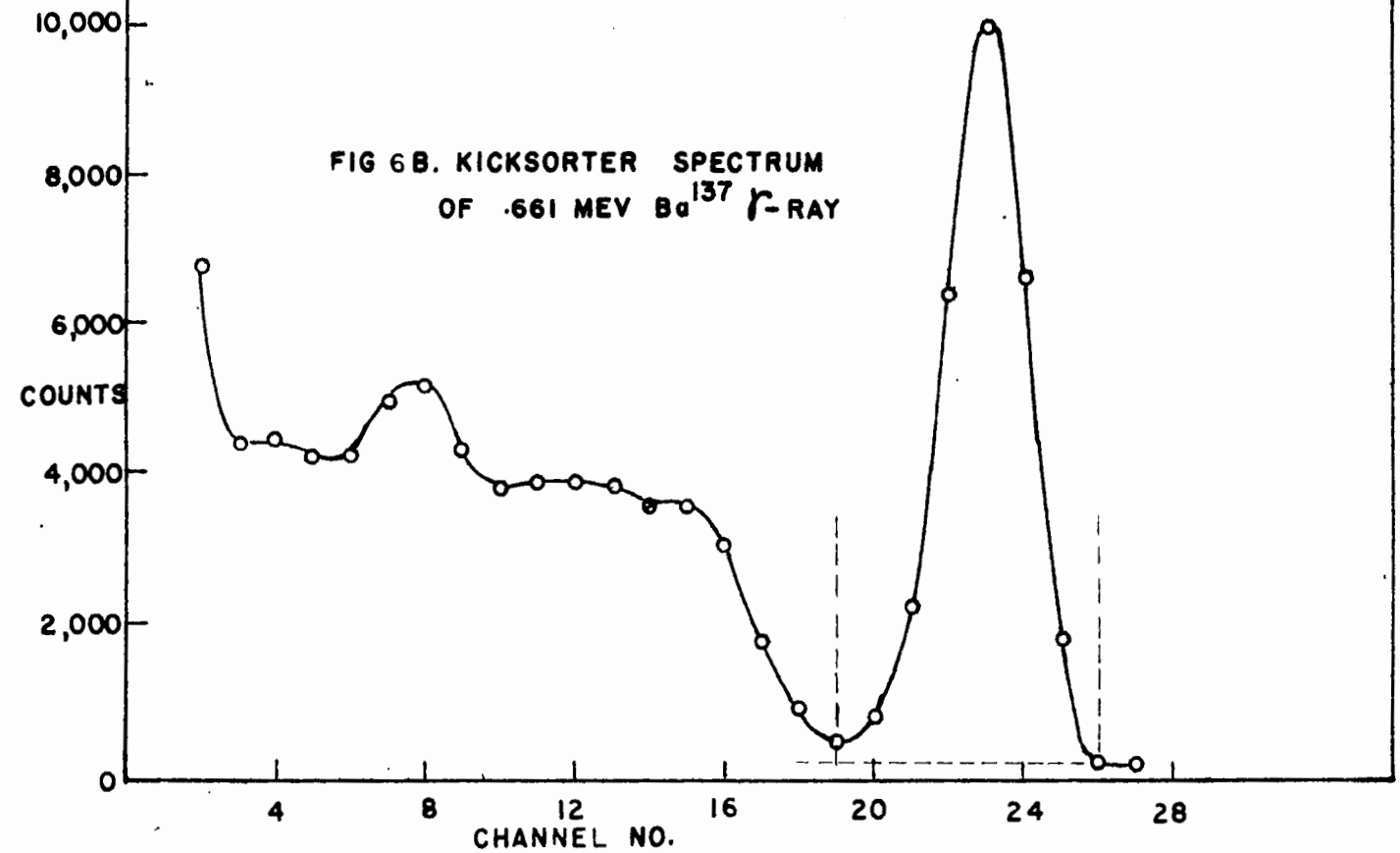

FIG 6 B. KICKSORTER SPECTRUM OF .661 MEV Ba^{137} γ-RAY

the .661 mev gamma ray is due largely to Compton absorption in the crystal. The Compton continuum is separated by a valley from the full energy peak and the resolution is 11%. (For a thicker crystal the relative number of continuum events to full energy events would be reduced.) There is a small peak superimposed on the Compton continuum and having its maximum between channel 7 and 8. It is caused by back-scatter quanta from the surface of the photomultiplier which are subsequently absorbed in the crystal. The energy resolution for the .074 and .661 mev gamma rays varies more slowly than inversely as the square root of the energy and suggests the presence of non-uniformity effects.

In general, the full energy pulse height for a NaI(Tl) scintillation counter increases linearly with the energy of the gamma ray. In particular, this has been found to be the case for the counting system shown in Fig. 5, at least above about 15 kev. Thus, if the kicksorter is properly set up, the energy corresponding to successive channels increases linearly with channel number. For a particular photomultiplier voltage and amplifier gain setting, the energy calibration of the kicksorter can be obtained with two or more sources of gamma rays of known energy which give a full energy peak in the range of the kicksorter. Fig. 7 shows a typical energy calibration resulting in a straight line function for energy versus channel no. Along the abscissa are indicated the gamma ray energies used and the interpolated channel no. at which they were observed to produce a full energy peak. The discriminator bias for the kicksorter was so set up that the energy calibration curve should pass through zero. The fact that it does not may indicate that the pulses are superimposed on a low amplitude level of noise.

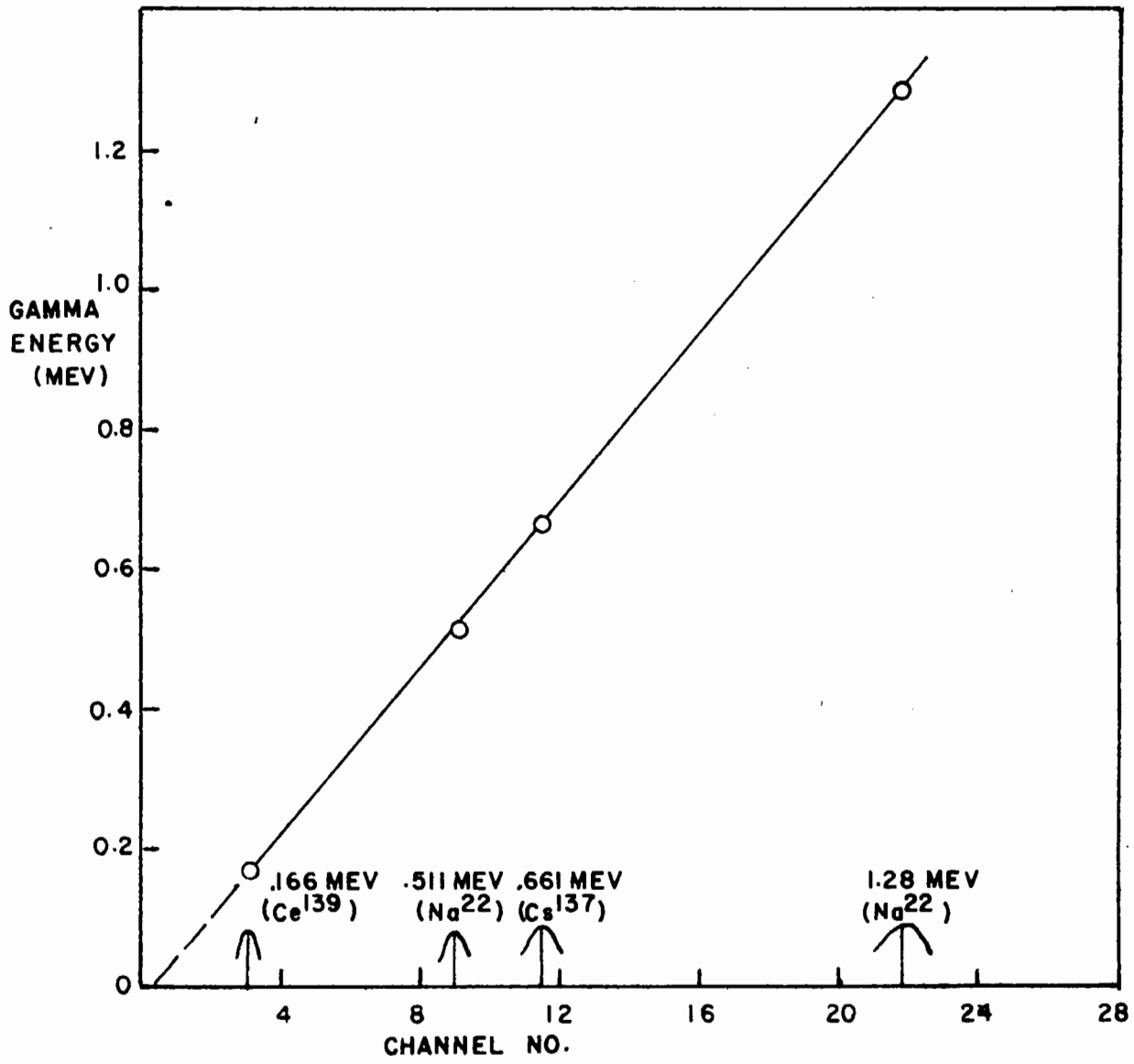

FIG 7. ENERGY CALIBRATION OF KICKSORTER

It is important to use comparable counting rates which are not too high (about 2000 total counts per sec, say) in calibrating the energy and in energy determinations, as otherwise d.c. shifts in bias levels may reduce the accuracy. In this work, however, energy accuracy was not of primary importance. It was only necessary to identify the x or gamma ray responsible for an observed peak.

In the determination of reaction yields from the decay of a particular x-ray or gamma ray, the photomultiplier voltage (continuously adjustable) and amplifier gain are set so that the full energy peak is conveniently within the range of the kicksorter. The photomultiplier voltage is adjusted so that the peak occurs decisively in a certain channel and the manually operated switch is set to read the voltage output of this channel, Beginning with all channels cancelled and reading zero volts output, count-sorting is carried on for a period of sufficient duration to give full scale deflection of 100V. in the peaking channel. The count is then stopped and the final spectrum is recorded on the Esterline-Angus recorder. The plotted counting rate is then the sum of all pulses making up the full energy peak divided by the time duration of the count. As it is the area of the peak that is involved, the accuracy of the measured counting rate is not affected by small changes in d.c. voltages which affect the position of the peak.

Generally, for changes in bombardment energy and as the activity decays, the shape of the background on which a peak is superimposed changes and the subtraction of it must take this into account. This was especially important for gamma rays above about 0.2 mev. Consistency in the subtraction of background could best be obtained by fitting the resulting peak to its

characteristic Gaussian shape. To do this, the particular gamma ray was, for each count sorting, made to peak in the same channel and its Gaussian shape and the total counts corresponding to 100V. peak height were either measured directly or interpolated from measurements on gamma ray standards. If the peak in question was clearly resolved it was usually sufficient to adjust the subtracted background (assumed to be smooth) for the peaking channel and the channel on either side of it so that the net side channel heights, made approximately equal by adjusting the photomultiplier voltage, and the net peak height fitted the measured Gaussian shape. Thus, the background had only to be found for three channels and with the peak made symmetrical with respect to the side channels the detailed shape of the background was not required to be known. Fig. 8 reproduces an Esterline-Angus histogram showing the .374 mev gamma ray emitted in the decay of isomeric lead (Pb^{204m}). The chosen background shown for channels 16, 17 and 18 gives net heights for these channels which fit the measured Gaussian. The peak height is 7500 counts and the measured total counts in the peak for a peak height of 10,000 counts was 23,800 counts. The count-sorting duration for the spectrum in Fig. 8 was 122.0 sec. The counting rate for the .374 mev peak is therefore

$$\frac{7500}{10,000} \times \frac{23,800}{122.0} = 146 \text{ counts/sec.}$$

(Channels 3, 4 and 28 have been filled to saturation of the amplifiers in their integrating circuits and therefore only give partial information. Channel 28 accepts all pulses larger than its discriminator level and so commonly goes into saturation.) The method of Gaussian fitting has also been used where the peak in question is not well resolved from another

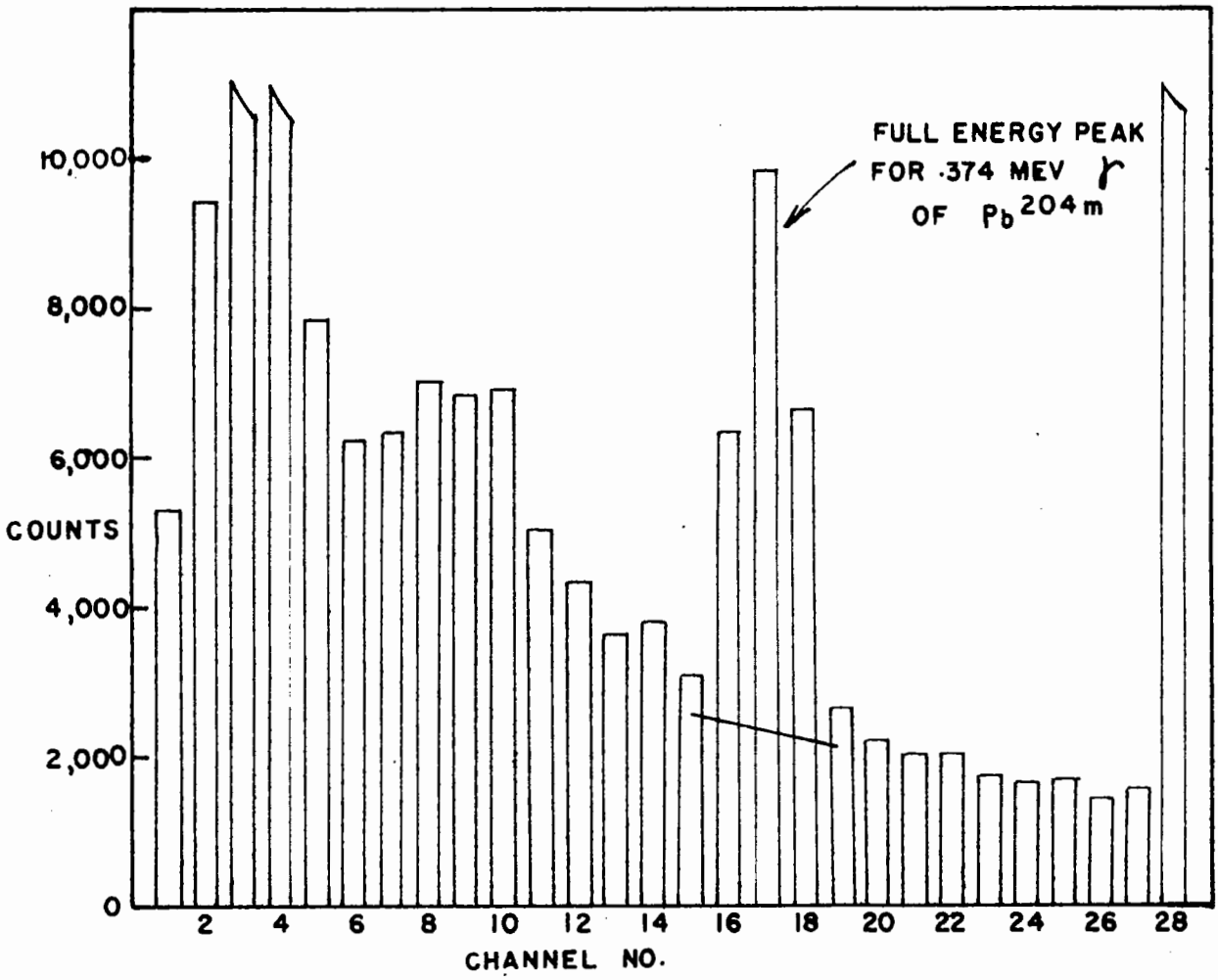

FIG 8. SUBTRACTION OF BACKGROUND BY GAUSSIAN FITTING

near it in energy. In this case the upper half scale is used so that the resolution of the instrument is better, and the portion of the peak which is unaffected by the interfering one is fitted to its Gaussian by proper choice of the background.

(c) Efficiency Calibration of NaI(Tl) Counter

The counter which was calibrated was that specified in Fig. 5, consisting of a 1 1/2" diam. by 1" high NaI(Tl) crystal mounted on a DuMont 6292 photomultiplier tube.

The efficiency e_p of the crystal for counting events in the full energy peak was determined as a function of distance from the source to the near surface of the crystal for gamma rays of energy 1.28, .661, .511 and .166 mev. Sources of known strength of Na^{22}, Cs^{137} and Ce^{139} were employed. For energies below about .1 mev, the computed total counting efficiencies of McGowan were used[27]. At these energies the absorption of the gamma ray is predominantly by the photoelectric process so that the full energy peak, together with the escape peak, comprise practically the total count. The values computed and tabulated by McGowan were for a NaI(Tl) crystal of the same shape and size as that calibrated in this work.

The efficiencies so obtained are tabulated in Table I. versus energy and distance. From this table, curves for efficiency versus energy at various fixed distances are given in Fig. 9 on a log-log plot. For energies up to about .1 mev the absorption is almost entirely by the photoelectric process and the one inch thick crystal absorbs nearly all the gamma radiation incident upon it so the efficiency varies only slowly.

E (mev) / d (cm)	.031	.048	.075	.166	.511	.661	1.28
0	.500	.500	.500				
1	.261	.265	.260	.206	.0354		.0093
2	.133	.136	.132	.104	.0188	.0134	.00516
3	.0754	.0771	.0750	.0570	.0117	.00780	.00292
4						.00510	
5	.0320	.0325	.0318	.0250	.00500	.00346	.00140
7	.0172	.0174	.0171	.0143	.00286	.00204	.00084
10	.0871	.00880	.00869	.00730	.00151	.00107	.000458
15				.00330		.000515	.000228
20	.00224	.00225	.00223	.00200	.000450	.000303	.00129
50	.000361	.000362	.000361				

Table I. NaI(Tl) Counter Efficiencies for Full Energy Events (for Counter in Fig. 5)

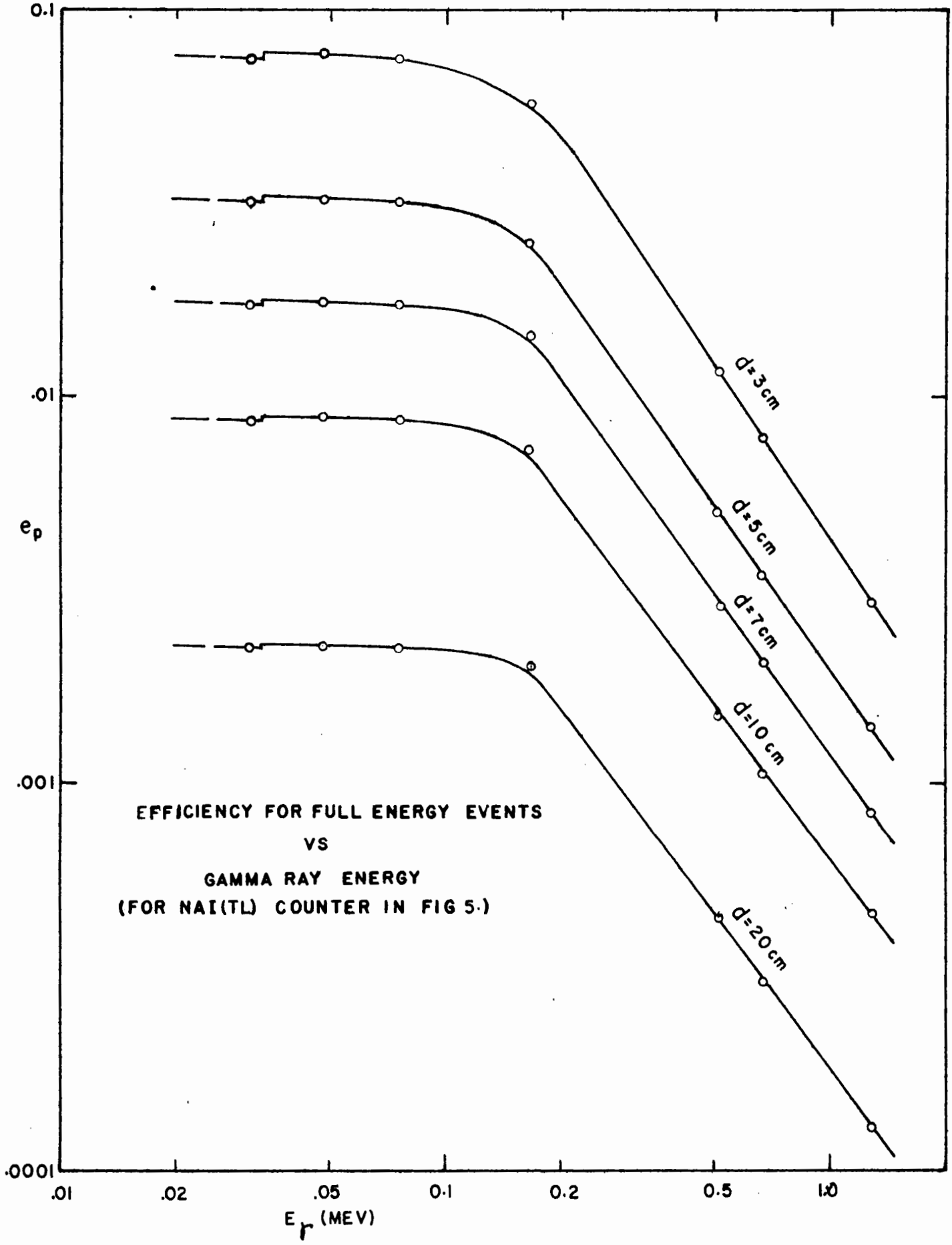

FIG 9. EFFICIENCY CALIBRATION FOR NAI(TL) CRYSTAL COUNTER

There is a small discontinuity at an energy of 33 kev where the K absorption edge for iodine occurs. Above 0.1 mev the Compton process begins to be important and the total absorption coefficient becomes smaller so that only part of the incident gamma radiation is absorbed in the crystal. Both these effects together cause the full energy efficiency to decrease rapidly with increasing energy.

By using the tabulated efficiencies (Table I) or the curves in Fig. 9, a kicksorter full energy counting rate for a particular gamma ray determines its absolute rate of emission if its energy and the distance from the source to the near surface of the crystal are known. It is emphasized that full energy events are here taken to mean those events resulting in the peak at full energy plus those giving the escape peak, if any.

4. Factors Entering into Absolute Cross Section Determination

(a) Ratio of K- to Total-Electron Capture

In order to know this ratio exactly it is necessary to know the disintegration energy available for the capture process. Of lesser importance is the degree of forbiddenness of the orbital capture decay. Since the neutrino energy can not be observed and mass differences from closed cycles and (p,n) thresholds are still scarce, the disintegration energy is rarely known.

Brysk and Rose[28] have investigated the theoretical transition probabilities for orbital capture in various shells. Wave functions for the bound state electrons were corrected for the finite size of the nucleus and for the effect of screening. The calculations show that, at disintegration energies appreciably above the K-capture threshold,

the K-capture fraction of the total is only a slowly varying function of energy. Also, by far the greatest single competition is from the L_I sub-shell at energies appreciably above its threshold. For disintegration energies well above the K-capture threshold, the ratio of L_I- to K-capture varies only slowly with energy; more highly forbidden transitions give successively higher L_I/K ratios, especially toward low disintegration energies. Near the K-capture threshold L_I capture becomes a rapidly changing function of energy.

The ratio of K- to total-electron capture used in the determination of cross sections for lead and bismuth was obtained from the theoretical results for an allowed transition by assuming an energy of disintegration of just the rest mass of the captured electron less its binding energy. This is equivalent to assuming a zero energy separation between states of neighboring isobars. The fact that there is little competition to electron capture from positron emission in this mass region indicates that the energy separation is seldom more than 0.5 Mev. The theoretical L_I/K ratio for $Z = 83$ and an allowed transition is then 0.21 and the L_{II}/K ratio is .02. L_{III}-capture is generally negligible except in the case of a first forbidden unique transition when it may be of the order of roughly 20% of the L_I fraction. By assuming that the transition probability varies as the inverse cube of the principal quantum number n, the contribution of higher shells was estimated at about 10% of the K-capture fraction. Thus a K- to total-capture ratio of 1/1.33 was obtained.

Only for disintegration energies near the K-capture threshold should this ratio be seriously in error and so it is expected that for the

majority of decays it is applicable. Cross sections obtained should be considered as most probably unaffected appreciably by the indeterminate nature of this factor but as lower limits in magnitude if they are.

(b) Internal Conversion K x-rays

The contribution to the K x-ray yield by internal conversion events can be calculated if the energies, branching intensities and multipolarities of all gamma rays are known. The number of internal conversion K x-rays per disintegration is then $f \sum_i (\alpha_K)_i \, q_i$ where f is the fluorescence yield, q_i is the fractional number of emitted gamma rays per disintegration, $(\alpha_K)_i$ is the K-conversion coefficient and the summation is over all gamma rays associated with the electron capture which show the same half life.

Failing such a detailed knowledge of the decay scheme the contribution of internal conversion K x-rays may be measured for all internal conversion events occurring within about 0.5 μsec of the capture x-rays. This is accomplished by the "summing" technique. When two K x-rays are absorbed by the crystal within a time of 0.5 μsec a pulse equivalent to the sum of their energies is produced. The "summing" peak due to such events varies in intensity as the square of the counter efficiency and is therefore easily recognizable if there is appreciable cascading of x-rays. Measurement of its intensity relative to that of the single x-ray peak leads to the information desired. Thus, if N is the disintegration rate, f the fluorescence yield, and k is the ratio of K to total electron capture, then the observed K x-ray counting rate is

$$N_K = N \, f \, e_p \left[k + \sum_i (\alpha_K)_i \, q_i \right] \qquad 2.6$$

where e_p is the counter efficiency. The counting rate for "summing" events is

$$N_{KK} = n\ f\ e_p\ k\ f\ e_p \sum_i (\alpha_K)_i\ q_i \qquad 2.7$$

The measured ratio is then

$$\frac{N_{KK}}{N_K} = k\ f\ e_p \frac{\sum_i (\alpha_K)_i\ q_i}{k + \sum_i (\alpha_K)_i q_i} = .71\ e_p \frac{\sum_i (\alpha_K)_i q_i}{.75 + \sum_i (\alpha_{Ki})\ q_i} \qquad 2.8$$

where the values k = 1/1.33 and f = 0.95 for lead have been inserted. The number of internal conversion K x-rays per disintegration is determined from rewriting 2.8 and multiplying through by f

$$f \sum_i (\alpha_K)_i q_i = 0.95 \cdot \frac{.75\ \frac{N_{KK}}{N_K}}{.71\ e_p - \frac{N_{KK}}{N_K}} = \frac{\frac{N_{KK}}{N_K}}{e_p - 1.40\ \frac{N_{KK}}{N_K}} \qquad 2.9$$

This expression neglects the occurrence of higher order "summing" events which involve higher powers of the counter efficiency and are not important in any case unless there are several intense and highly converted cascading gamma ray transitions associated with the electron capture.

In practice the sum peak is first identified by observing its intensity relative to the K x-ray peak as a function of counting efficiency. Then, at source to counter distances where the efficiency e_p is well-known and the ratio N_{KK}/N_K is accurately measureable, the value of $\sum_i (\alpha_K)_i\ q_i$ is calculated. It is usually necessary to compromise between the two factors as for close distances and a high ratio of N_{KK}/N_K the efficiency is not so well-known since it depends more critically on the size, positioning and thickness of the active sample.

(c) Fluorescence yield

The fluorescence yield is defined for the K-shell as

$$\omega_K = \frac{X_K}{V_K} = \frac{X_K}{A_K + X_K} \qquad 2.10$$

where X_K is the number of K vacancies resulting in K x-rays

A_K is the number of K vacancies resulting in K Auger electrons

V_K is the number of primary vacancies in the K shell.

Experimental measurements of ω_K plotted as a function of the atomic number Z have been reproduced, for example, by Bergstrom[29]. For lead the measurements give $\omega_K = 0.95$.

(d) Self-absorption in Active Sample

Lead samples used were about 80 mg/cm^2 in thickness. Assuming that the effective absorber thickness was half the thickness of the sample, the measured attenuation through an 80 mg/cm^2 Pb absorber gave a self-absorption for the sample of 7%. This agrees very well with the calculated attenuation due to 40 mg/cm^2 using a total absorption coefficient for 74 kev photons in lead of 2.0 cm^2/g.

(e) Complete expression for the Cross Section

Rewriting equation 2.4 for the cross section for a particular reaction we have

$$\sigma = \frac{c\, A_i}{\lambda\, n\, p} \qquad 2.4$$

The constant c for lead can now be written explicitly in terms of the factors discussed above

$$c = \frac{1}{e_p} \times 1.33 \times \frac{1}{1 + f \sum_i q_i\, (\alpha_K)_i} \times \frac{1}{0.95} \times \frac{1}{0.93}. \qquad 2.11$$

III. EXPERIMENTAL MEASUREMENTS AND DISCUSSION OF RESULTS

1. Choice of Element for Study

Successive (p,xn) cross section measurements, employing the methods used in this work, are limited to those elements for which the various reactions lead to radioactive products with not too extreme half-lives. It is, in addition, desirable for the element being studied to have only one isotope of any appreciable abundance.

The (p,xn) cross section measurements by Bell on bismuth (Fig. 3), including the (p,2n) measurements by Kelly, suggested that there may be an odd-even effect whereby reactions involving the emission of an even number of neutrons are favoured over those in which an odd number are emitted.

It then seemed profitable to study (p,xn) cross sections in Pb^{206} for several reasons. The uranium radioactive series ends with this isotope of lead and so it is possible to obtain lead consisting predominantly of Pb^{206}. The radiogenic material used contained 88.2, 8.7 and 3.1 per cent respectively of the lead isotopes 206, 207 and 208; it came originally from Eldorado Mining and Refining (1944) Ltd. Now, (p,xn) reactions in Bi^{209} and Pb^{206} involving the emission of an even number of neutrons yield product nuclei which are respectively even-even and odd-even and so it seemed of interest to determine whether or not the odd proton would alter the nature of the anomalous results observed for bismuth. If they were explainable by some gross-structure effect such as nuclear size, the nature of the fluctuations should be altered only slightly in going from Bi^{209} to Pb^{206}. A study of Pb^{206} seemed additionally attractive since (p,xn) reactions lead to electron

capture decays of convenient half lives. For a few of the isotopes produced, however, successive reactions lead to decays with about the same half-lives and it is difficult to determine the respective yields.

The quantity actually measured, for the radiogenic mixture bombarded, is the cross section per atom of lead for production of a certain radioactive product. The same product nucleus can result from a (p,xn), (p,(x + 1)n), (p, (x + 2)n) reaction in Pb^{206}, Pb^{207}, Pb^{208} respectively. The cross section for Pb^{206} was accordingly obtained by subtracting the relatively small contributions by Pb^{207} and Pb^{208} to a particular yield, on the assumption that the (p,xn) cross sections in these isotopes were identical to those for Pb^{206}.

2. Successive (p,xn) Cross Section Measurements in Pb^{206}

Fig. 10 shows the section of the periodic table involving the Pb^{206} (p,xn) reaction products, the cross sections of which were measured. The mode of decay and half-life for each product and daughter are indicated. The energies in Mev of some of the gamma rays are given and those used for relative or absolute cross section determinations are circumscribed. Data is taken from the tables of Hollander, Perlman and Seaborg[30] unless it is otherwise noted in the discussion.

(a) (p,n) Bi^{206} (6.4 days)

The absolute yield of active Bi^{206} atoms was determined from the decay curve for the K x-rays. Relative yields at various bombarding energies could be obtained from the decay curve of a composite full energy peak due to three gamma rays of energy .803, .881 and .895 mev. The sum of the transition intensities of these three gamma rays is given by Alburger and Pryce[31] as about 1.75 per disintegration of Bi^{206};

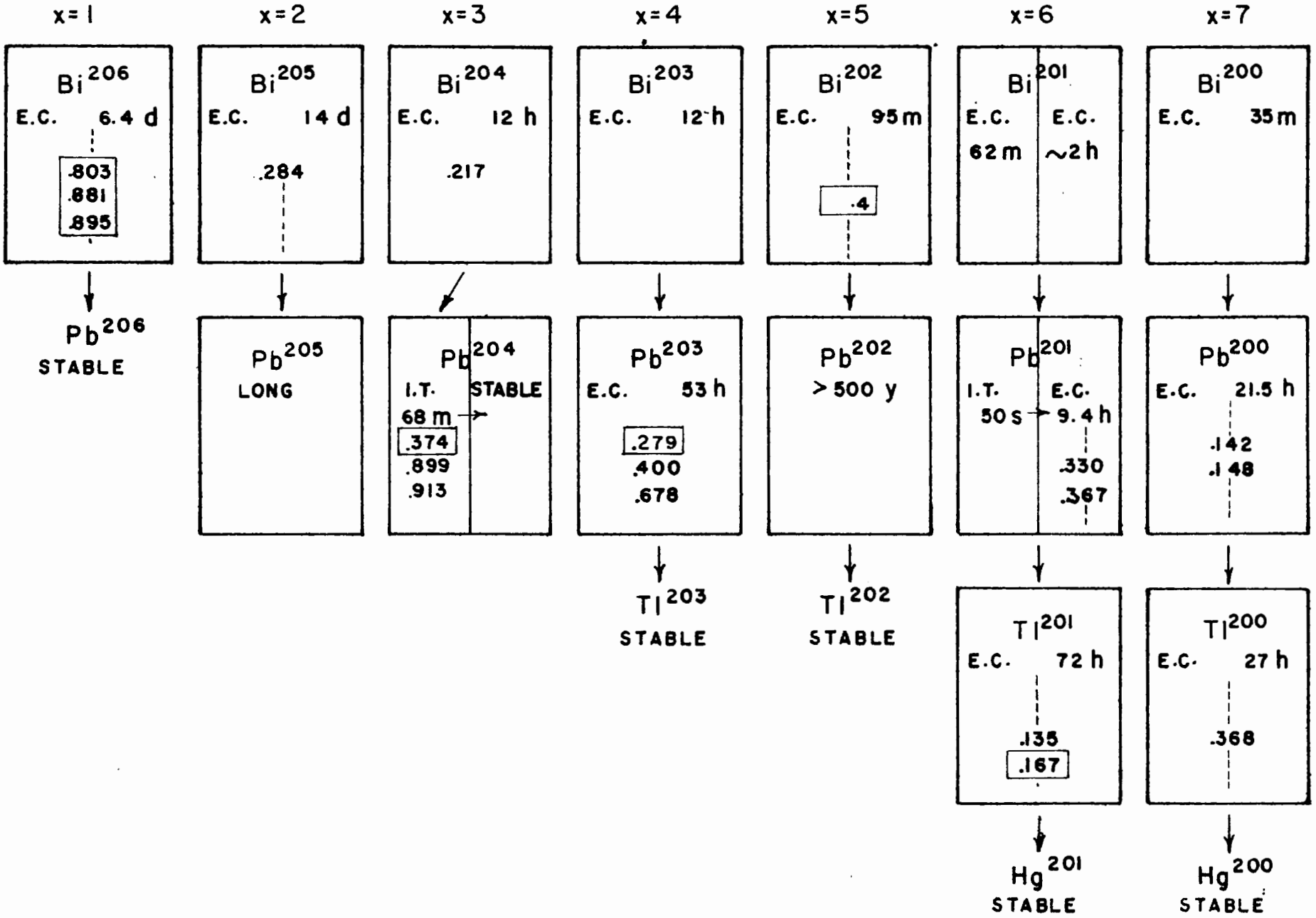

FIG 10. DECAY OF $Pb^{206}(p,xn)$ REACTION PRODUCTS

from the same work it is seen that internal conversion of the many gamma transitions gives $f \sum_i (\alpha_K)_i \, q_i = 0.45$. Using these values, the absolute yields from the K x-ray activity agree well (within 5%) with the absolute yields determined from the gamma ray group.

(b) $(p,2n)Bi^{205}$ (14 days)

The decay of the K x-ray activity was used exclusively in the determination of the yield of this reaction. While there are some prominent gamma rays following the electron capture in Bi^{205}, the changing background (due to shorter lived gamma rays) upon which they were superimposed made it difficult to use them for a prompt determination of the relative yield. However, as the half-life of 14 days is long compared with the half-lives of activities due to other (p,xn) reactions, it was only necessary to wait long enough in order to obtain a pure 14 day x-ray activity. The (p,2n) cross section could therefore be determined over a wide range of bombardment energies.

An attempt was made to measure the ratio of L-capture to K-capture for a pure 14 day Bi^{205} activity. The active bismuth was chemically separated and deposited between two thin VYNS films by Dr. L. Yaffe of the McGill Chemistry Department. The sample thickness was about 2 mg/cm^2. A special crystal counter was assembled with a thin (16.6 mg/cm^2) cover of aluminum over the end face of the NaI crystal. The L x-rays of Pb (11 kev) could then be distinguished from the noise as a distinct peak on a kick-sorter spectrum containing the K x-rays. Correcting for preferential absorption of L x-rays in the thin source and in the aluminum cover of the counter, the observed ratio of L to K x-rays led to an L to K capture ratio of about 0.4 ± 0.2. The large probable error is due only partly to

error in the measurement of the relative intensities of the L and K x-rays. The fluorescent yield for L x-rays is not well known. Assuming a distribution of L sub-shell vacancies equal to that following the emission of K x-rays, the work of Kinsey[32] yields an effective fluorescent yield for L x-rays of about .36 for lead. This value was used and it was further assumed that 70% of the K x-rays leave vacancies in the L shell. The value of 0.4 ± 0.2 so obtained for the L- to K- capture ratio, as compared with the assumed value of 0.23, only indicates that for the decay of Bi^{206} an assumed K to total electron capture ratio of 1/1.33 is not grossly inaccurate, i.e., it is at least correct to within 20 percent. The factor 1/1.33 has therefore been used, keeping in mind that it may be an upper limit and that the (p,2n) cross section so obtained is probably a lower limit in magnitude. This conclusion is strengthened by considering that, for the same degree of forbiddenness of electron capture, the longer than average half-life of 14 days may indicate that there is a lower than average decay energy. This would lead to a higher L- to K-capture ratio.

(c) $(p,3n)Bi^{204}$ (12 hr) $\longrightarrow$ Pb^{204m} (68 min.)

Absolute yields of this reaction were based upon the 12 hr K x-ray activity in the decay of Bi^{204} to the 68 min. isomeric state in Pb^{204}. After this 68 min. state reaches equilibrium with the bismuth parent, gamma rays emitted in its decay are to be found which show a 12 hr half life. According to a scheme proposed by Bergstrom and Wapstra[33] the 68 min. state decays with the emission of a .913 mev E5 transition to a second isomeric state with a half-life of 0.3 μsec. This state then decays with the emission of a .374 E2 transition in cascade with a .899

mev E2 gamma transition to the ground state of stable Pb^{204}. This scheme is corroborated in this work inasmuch as the transition intensity of the .899-.913 mev group relative to that for the .374 mev gamma transition was measured to be 2.0. (This was obtained by observing the relative number of counts in the full energy peak due to the unresolved .899 and .913 mev gamma rays to the number in the .374 mev peak, and then applying the measured counter efficiencies and internal conversion corrections for the respective gamma rays.) The .374 mev gamma ray was used to obtain relative yields at various energies of bombardment. At energies above the threshold for the (p,4n) reaction, Bi^{203} is produced and decays also with a half-life of 12 hrs. It would therefore have been difficult to determine the respective yields of the (p,3n) and (p,4n) reactions entirely on the basis of the x-rays. Absolute cross sections for the (p,3n) reaction were corrected for a summing factor of $f\,\Sigma = .37$. The K x-ray contribution from prompt internal conversion accompanying electron capture in Bi^{204} was measured to be $f\,\Sigma_{(Bi^{204})} = .27$ and the contribution from gamma transitions in Pb^{204m} was calculated to be $f\,\Sigma_{(Pb^{204})} = .10$. Upon applying internal conversion corrections, absolute cross sections obtained from the .374 mev gamma ray intensity were then 5% higher than those obtained from the K x-ray.

(d) $(p,4n)Bi^{203}$ (12 hr.) $\longrightarrow Pb^{203}$ (53 hr.)

Due to the presence of the 12 hr Bi^{204} product of the (p,3n) reaction it was impossible to determine the (p,4n) yield accurately from the 12 hr decay of Bi^{203} x-rays. Therefore the absolute yield of the (p,4n) reaction was determined from the 53 hr daughter x-ray activity (Pb^{203}) remaining after the decay of the 12 hr isotopes. Since Pb^{203} can be produced

directly through a (p,p3n) reaction in Pb^{206} the cross section for (p,4n) is augmented by a small contribution from the reaction (p,p3n). The cross section was calculated assuming that the 53 hour activity was derived entirely from the parent Bi^{203}. Relative yields at various energies were got by observing the growth and decay of the .279 mev gamma ray activity following electron capture in the Pb^{203} daughter. Wapstra et al[34] have published a decay scheme in which this gamma ray is identified as a mixture of E2 and M1 and the only transition contributing appreciably to the internal conversion K x-rays. A K conversion coefficient of 0.14 and a total conversion coefficient of 0.20 are reported. In good agreement with these results, a summing experiment was performed on a nearly pure 53 hour activity and gave for the total number of "prompt" K x-rays due to internal conversion events per disintegration, $f \sum_i (\alpha_K)_i \, q_i = 0.14$. Upon suitable correction for internal conversion, the absolute yields determined from the .279 mev gamma ray agreed to within 10% with those determined from the x-rays. (The gamma ray gave cross sections which were about 10% higher). Fig. 11 shows the growth and decay curves measured for a sample bombarded at 39 mev. The initial activity of Bi^{203} is obtained by fitting the computed 12 hr $\longrightarrow$ 53 hr composite decay curve to the 53 hr tail of the x-ray decay and by fitting the computed curve for the 53 hr growth and decay curve to the measured points for the gamma ray. The points on the 53 hr x-ray tail were got by subtracting first the activity due to 14 day Bi^{205}.

The .279 mev gamma ray (in Tl^{203}) following electron capture in Pb^{203} also accompanies the beta decay of Hg^{203}. By comparing the ratio of the K x-ray intensity to the intensity of the .279 mev gamma ray for the lead

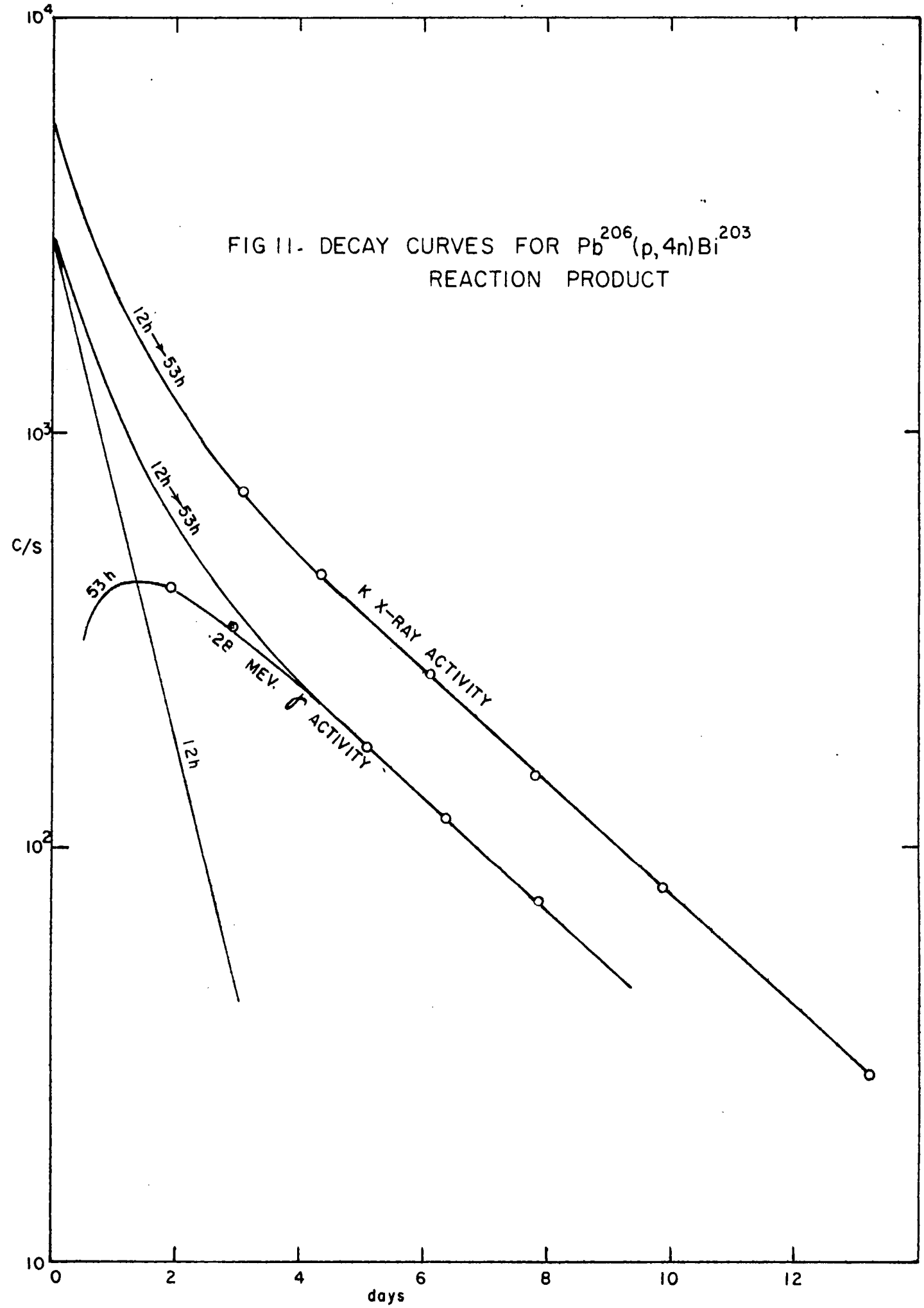

FIG 11. DECAY CURVES FOR $Pb^{206}(p,4n)Bi^{203}$ REACTION PRODUCT

and mercury decays, Wapstra et al[34] measured a value for the K- to total-electron capture ratio in Pb^{203} which is independent of the calibration of the scintillation counter. They obtained $\frac{1}{1.34 \pm 0.1}$, in excellent agreement with the value 1/1.33 assumed in this work.

(e) (p,5n) Bi^{202} (95 min.)

Absolute yields of this reaction were computed from the 95 min. K x-ray activity accompanying electron capture of Bi^{202} to long-lived Pb^{202}. A gamma ray peak of about 0.43 mev energy helped to determine relative yields where it was difficult to know the 95 min. fraction in the complicated x-ray decay. For bombardment energies up to the threshold for the (p,6n) reaction it was relatively easy to find the amount of 95 min. activity present in the gross x-ray decay curve since longer-lived activities due to (p,2n) (p,3n) and (p,4n) reactions were known accurately. It was only necessary to wait long enough in order to know the (p,2n) 14 day activity and the intensities of the .374 and .279 mev gamma rays indicated respectively the x-ray decay curves due to the (p,3n) and (p,4n) reactions. Above the (p,6n) threshold, however, Bi^{201} is produced and decays with a half-life similar to 95 min. Bi^{202}. Of the two states in which Bi^{201} is reported to be formed (see Fig. 10) the 2 hr. decay agrees best with the analysis of the complicated x-ray decay curve. Formation of a small amount of 62 min. Bi^{201} cannot however be excluded. This is not important with respect to yield determinations for the (p,6n) reaction as these were obtained by observing the 72 hr. grand-daughter activity in Tl^{201}. Fig. 12 shows an analysis of a complicated K x-ray decay curve into its several components. The 14 day activity was found by waiting until shorter lived activities decayed away. The 12 h (p,3n) and 12 h $\longrightarrow$ 53 h (p,4n) components were got from the respective intensities

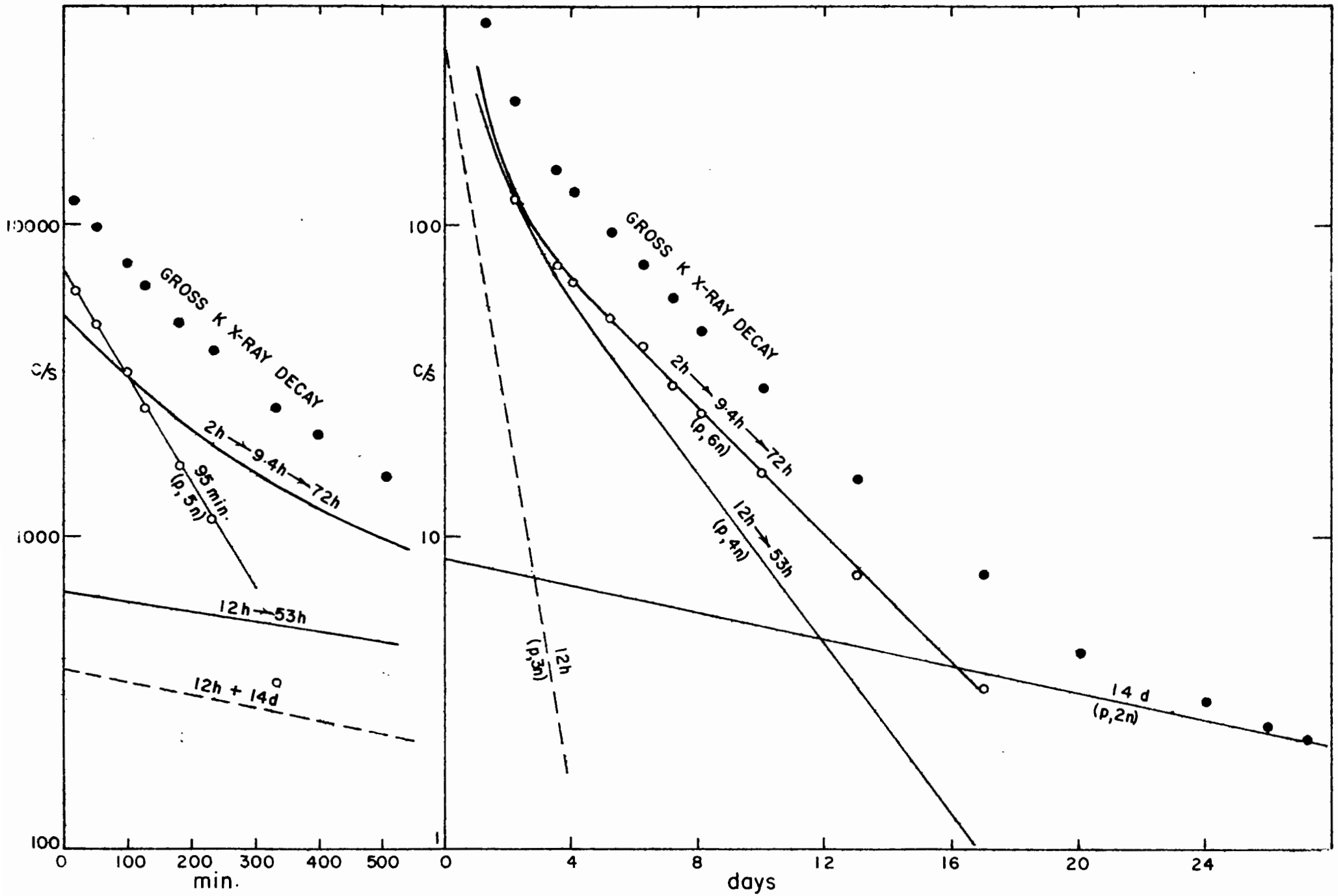

FIG 12. ANALYSIS OF K X-RAY DECAY

of the .374 and .279 mev gamma rays. (The 12 hr Bi^{204} activity is not so well known since the kicksorted .374 mev gamma ray peak contained an unresolved contribution from some longer lived gamma ray.) The residual activity then showed a good 72 h half-life over the period from 5 to 17 days after bombardment. The composite decay curve due to the (p,6n) reaction was computed assuming the decay 2h → 9.4h ⟶ 72h and fitted to the 72 hr. tail. The left portion of Fig. 12 shows the component activities which were subtracted from the gross K x-ray decay in order to obtain the 95 min. (p,5n) yield. Yields so obtained agree fairly well with those got from relative intensities, at various energies, of the 95 min. 0.43 mev gamma ray peak, although this peak was not well resolved from gamma rays of different half-lives.

A summing experiment was performed on a K x-ray source consisting mainly of 95 min. (p,5n) activity as well as known proportions of 12h → 53h (p,4n) and 12h (p,3n) activities. It was unfortunately difficult to measure the relatively high summing factor very accurately as the sum peak was unresolved from a gamma ray of about the same energy. This gamma ray appeared to decay with about a 95 min. half-life. The sum peak was corrected for the effect of the gamma ray by observing its intensity at large distances where summing is negligible. Then from the known proportions of the respective activities present and the known summing factors for the (p,3n) and (p,4n) activities, a summing factor of $f\,\Sigma = .35$ was obtained for the 95 min. (p,5n) fraction. As the gamma rays accompanying the decay of Bi^{202} had not been previously studied it was decided to investigate them in a rough manner by means of the kicksorter. Kicksorted pulse height spectra due to Bi^{202} gamma rays were observed and are shown in Fig. 13. Energy calibration of the kicksorter was carried out (as

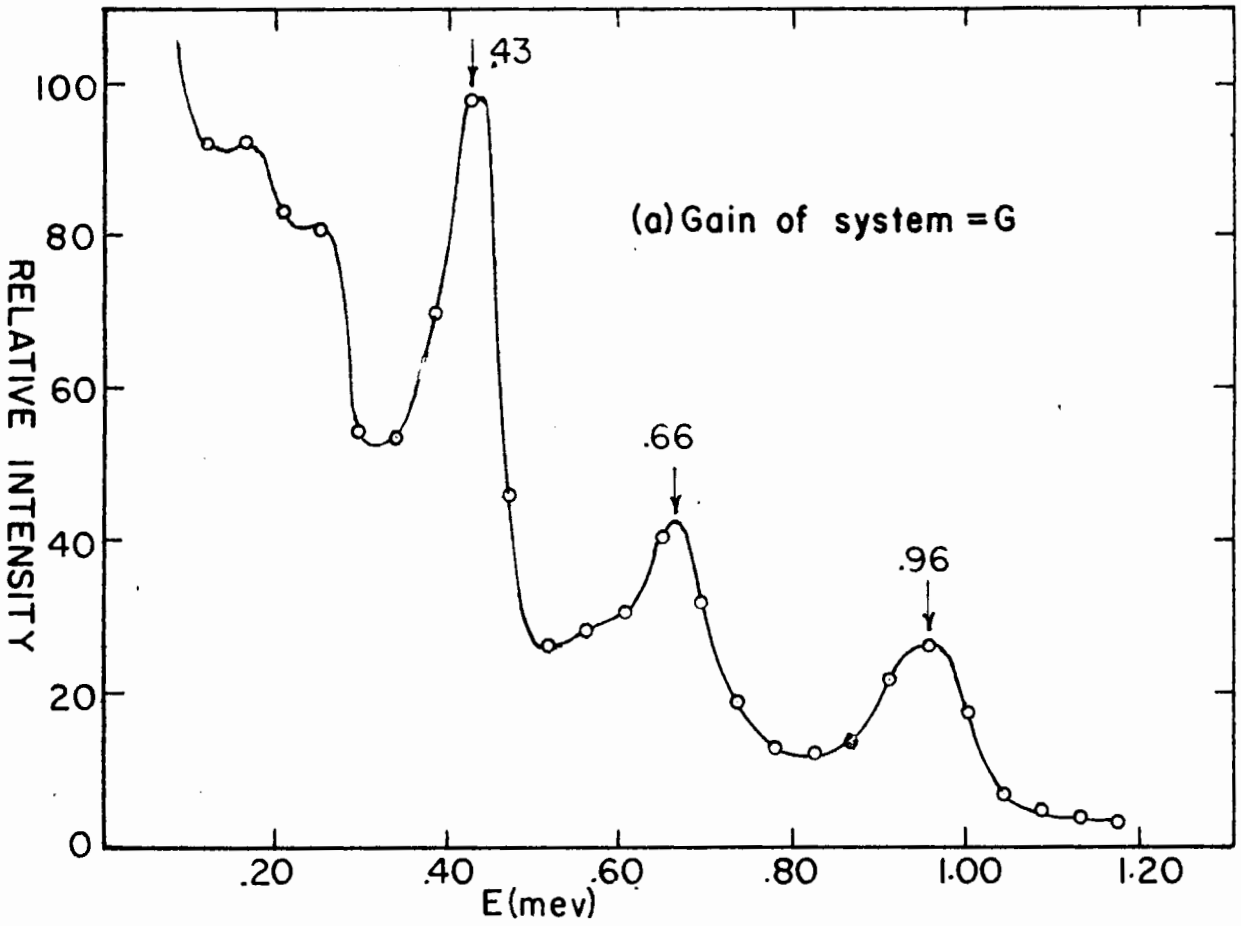

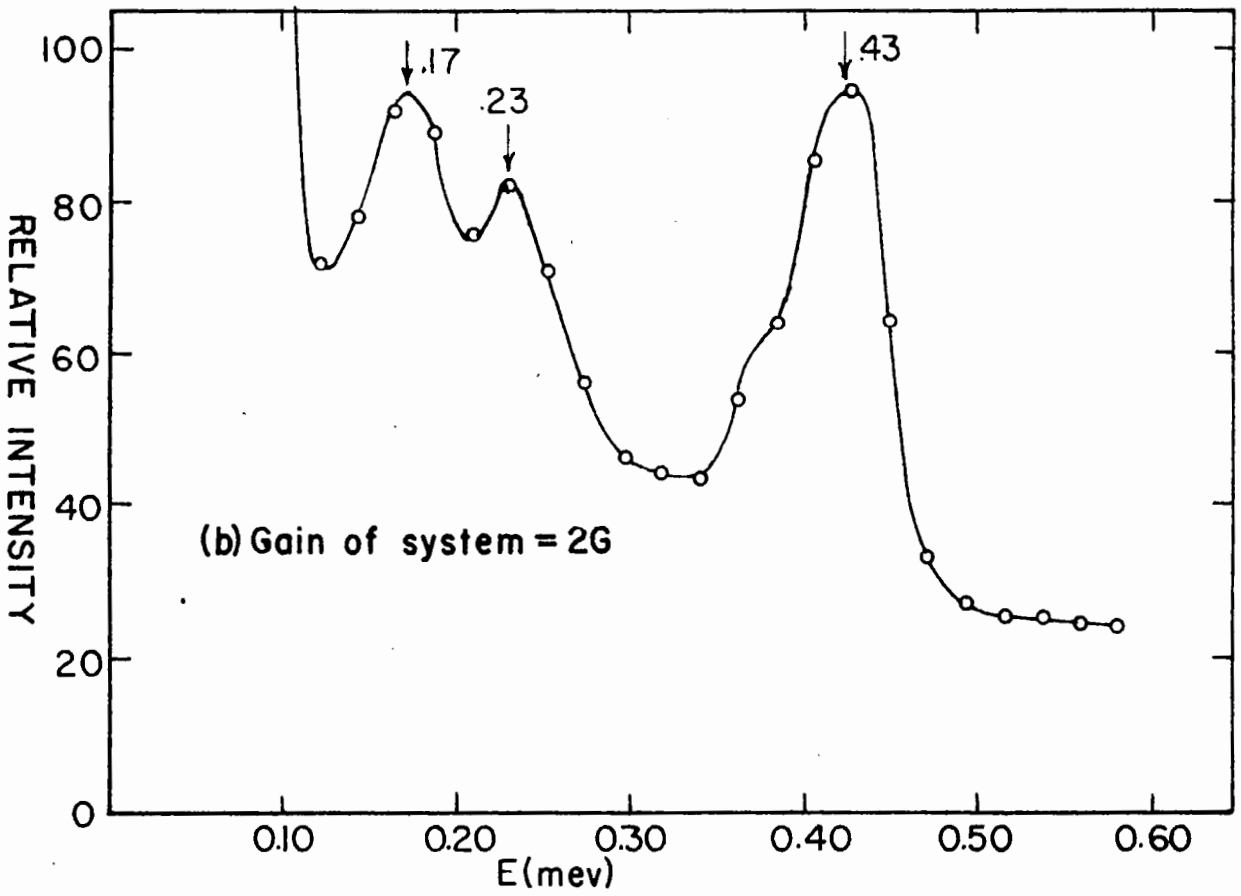

FIG 13. KICKSORTED PULSE HEIGHT SPECTRA OF Bi^{202} γ RAYS

described in II. 3.(b)) for each gain setting with the aid of sources of gamma rays of known energies. Peaks showing a 95 min. decay were observed in channels corresponding to energies of .17, .43, .66 and .96 mev (to within about 3%). Fig. 13(b) shows that the .43 mev peak is a composite formed from at least two gamma rays. The ratio of (p,5n) to (p,3n) + (p,4n) K x-ray activity in the active source was about 3 to 1 at the time the spectra were observed. There may therefore be some contribution from gamma rays emitted in the decay of Bi^{203} and Bi^{204}. A small peak at about .23 mev may possibly be the .217 mev gamma ray reported to accompany the decay of Bi^{204}.(30)

(f) (p,6n) Bi^{201} (2 hr; 62 min) $\longrightarrow$ Pb^{201} (9.4 hr) $\longrightarrow$ Tl^{201} (72 hr)

The yield of this reaction, as noted above, was computed from the 72 h grand-daughter x-ray activity, Tl^{201}. Its growth and decay was assumed to derive from the series Bi^{201} $\xrightarrow{2h}$ Pb^{201} $\xrightarrow{9.4h}$ Tl^{201} $\xrightarrow{72h}$ Hg^{201} (stable). The half-life for Pb^{201} was taken as 9.4h, as indicated by the work of Bergkvist et al(35). It is apparent that yields determined from the 72h Tl^{201} activity depend very little on whether Bi^{201} decays with a half-life of 62 min. or 2h or with a mixture of the two. However, 72h Tl^{201} can derive from (p,p5n) and (p,2p4n) reactions as well as from a (p,6n) reaction in Pb^{206} and so the resultant cross section represents approximately the sum for the three reactions. The fact that a different radioactive series characterizes the 72h activity for each reaction was neglected and the cross section was calculated assuming the series for (p,6n). Fig. 12 shows a determination of the 72h activity obtained by subtracting the known (p,2n), (p,3n) and (p,4n) components. By fitting the composite decay curve for 2h $\rightarrow$ 9.4h $\rightarrow$ 72h to the 72h tail the cross section is computed from the initial 2h activity. Above the threshold

for the (p,7n) reaction it was difficult to determine accurately the amount of 72h x-ray activity present. The (p,6n) cross section was therefore computed from the relative intensity of a 72 hr. .167 mev gamma ray of weak intensity (about .05 per disintegration).

A summing experiment was performed on an x-ray source consisting of known proportions of 72h, 53h and 14d activities. The accuracy was limited due to the fact that the sum peak was not well resolved from the .167 mev gamma ray peak. A value of $f \sum_i (\alpha_K)_i \ q_i$ of 0.15 was observed for the 72h fraction. This agrees well with the value of 0.17 calculated from the relative K-line intensities for the .135 mev M1 and .167 mev M1 gamma transitions[35] and the measured intensity per disintegration of the .167 mev gamma ray.

(g) $(p,7n)Bi^{200}(35\ min) \rightarrow Pb^{200}(21.5\ hr) \rightarrow Tl^{200}(27\ hr)$

The cross section for this reaction was determined at only one bombardment energy,- 64 mev. It was determined from the initial 35 min. Bi^{200} x-ray activity which was found by subtracting from the gross x-ray decay curve the components due to (p,3n), (p,4n), (p,5n) and (p,6n) reactions. The value so obtained therefore depends on the assumption that Bi^{201} decays entirely via the 2h state.

As relatively large amounts of 95 min Bi^{202} and 2h Bi^{201} activities were present it was difficult to determine the number of internal conversion K x-rays per disintegration of the 35 min. activity from the summing technique. This is due to the large value of this factor for gamma rays accompanying the decay of Bi^{202} and the unknown value of it for the decay of Bi^{201}. Accordingly, no correction for internal conversion was applied to the cross section value. In absolute value, therefore, it is somewhat less reliable than cross sections for the other (p,xn) reactions.

3. Experimental Errors

By estimating the relative dispersion $\left(\frac{\text{standard deviation}}{\text{mean value}}\right)$ for each of the measured factors involved, it is possible to give a value for the relative dispersion in the absolute cross sections tabulated in Table II. Rewriting equation 2.4 for the cross section of a particular reaction we have

$$\sigma = \frac{c\ A_i}{\lambda\ n\ p} \qquad 2.4$$

The estimated relative dispersions are, for

A_i = 5%

n = 5%

p = 10% (estimated from the separate errors involved in the expression for p, eq. 2.5)

c = 8%

The relative dispersion for c was arrived at by estimating the relative dispersions for e_p and $\frac{1}{1 + f \sum_i (\alpha_K)_i\ q_i}$ as 7% and 4% respectively.

By summing the squares of the individual relative dispersions and taking the square root of the total one obtains a relative dispersion for σ as follows

$$\sqrt{2\ (5^2)\ +\ 10^2\ +\ 8^2} = 15\%$$

It is to be emphasized that this estimate only allows for random errors which occur in the experimental measurements made. The indeterminate nature of the K- to total-electron capture ratio affects all the points for a given (p,xn) cross section by the same fractional amount, if it is different from the value 1/1.33 assumed. The fact that, for (p,n), (p,3n) and (p,4n) reactions, the absolute cross sections obtained from gamma rays agree within 5 or 10% with those based on the K x-ray intensity strongly

suggests that the K- to total-electron capture ratio is in fact close to 1/1.33 for these decays. For the (p,2n) reaction, the attempted measurement of the L/K capture ratio indicates that 1/1.33 may be an upper limit for K- to total-capture, making the cross section so obtained a lower limit. For the (p,5n), (p,6n) and (p,7n) cross sections there is no check on the ratio 1/1.33 assumed.

4. Discussion of Results

The measured cross sections for the successive (p,xn) reactions in Pb^{206} are tabulated in Table II and plotted against proton energy in Fig. 14.

With the exception of the (p,n) curve the cross sections reach a maximum value of the order of one barn. The curves rise rapidly with increasing energy beyond the apparent threshold and peak about 10 mev above it. On the high energy side of the peak the cross sections tail off to nearly constant values which, with increasing x, are progressively higher relative to the peaks. The (p,n) cross section is much less due to the much lower probability that the incident proton will penetrate the Coulomb barrier in this energy region; a maximum value of 0.25 barn is reached.

The shapes of the individual cross section curves are well explained by considering that a particular reaction proceeds either by particle evaporation from an excited compound nucleus or by a prompt internal cascade followed by particle evaporation. At the lower energies of bombardment, where the evaporation process is predominant (up to 30 or 40 mev), the cross sections peak sharply; the rapid rise with energy beyond the threshold and, following the peak, a subsequent rapid decrease

Proton Energy (Mev)	Pb^{206} Cross Sections (Barns)						
	(p,n)	(p,2n)	(p,3n)	(p,4n) +(p,p3n)	(p,5n)	(p,6n) +(p,p5n) +(p,2p4n)	(p,7n)
12.7	.23	.06					
16.3	.06	.53					
20.7		1.05	.02				
24.6		.98	.52				
25.0		.76	.54				
27.8		.53	.88				
27.9			.73				
28.0		.54					
30.0		.36	.89				
31.0			.77	.06			
34.0			.73	.37			
35.9		.15	.57	.49			
36.6			.40	.62			
39.2		.12			.02		
39.8				.91			
41.2			.15	1.11			
42.4		.13	.18		.14		
45.4		.16	.19	1.03	.37		
45.8				.97	.36		
49.0		.13	.14	.52	.57	.05	
52.5		.15		.47	.59	.26	
56.3		.11		.30	.38	.40	
63.8		.09		.21	.21	.55	.18

TABLE II. Pb^{206} (p,xn) Cross Sections

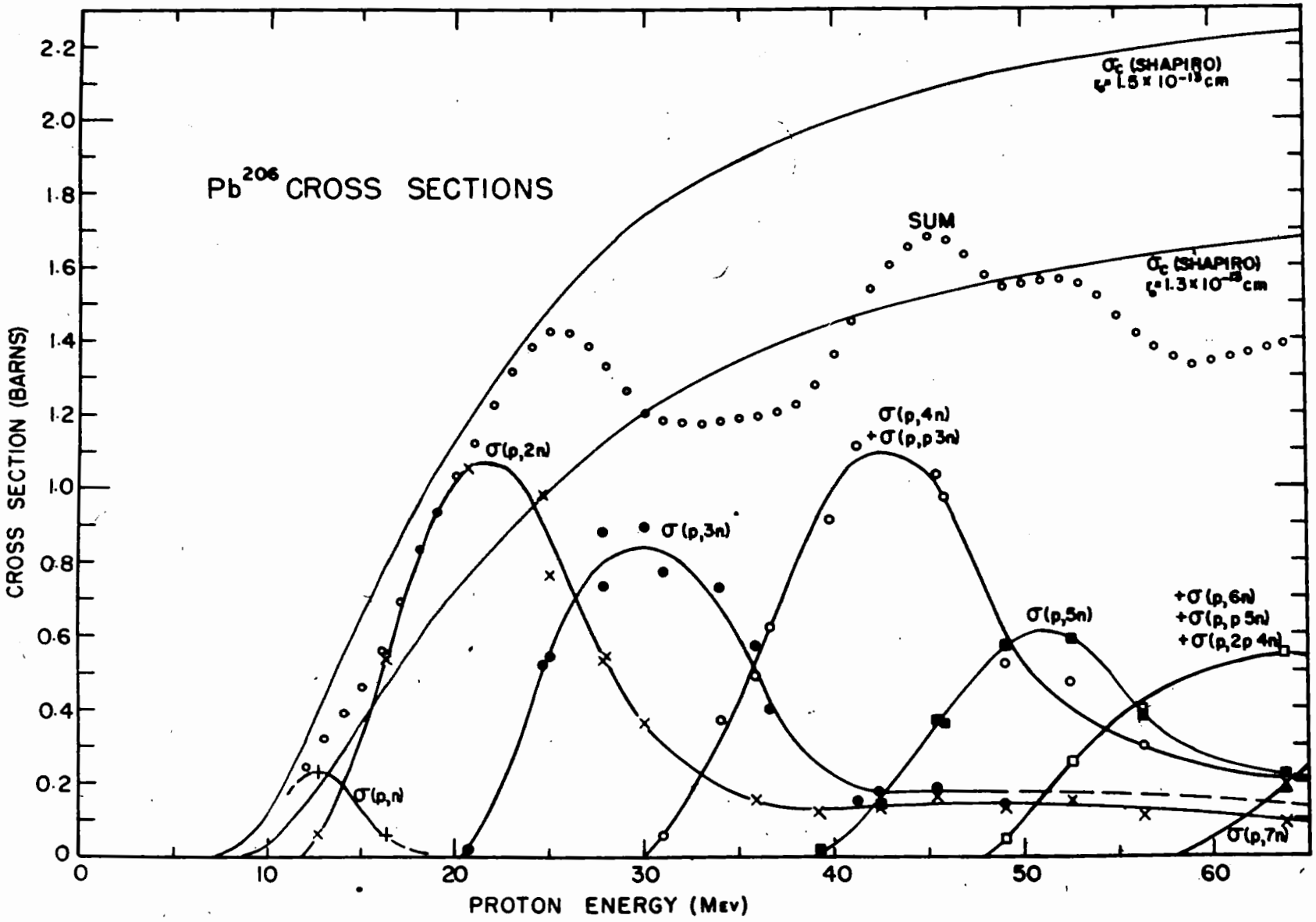

FIG. 14 MEASURED CROSS SECTIONS IN Pb^{206}

with the onset of an evaporation process involving emission of one more particle are characteristic. Toward higher energies and x values the evaporation peak is less sharp and internal cascade events become increasingly important. Cross sections for internal cascade reactions vary only slowly with energy and there are consequently a large number of reactions occurring at a certain energy. The general shape of each individual measured (p,xn) cross section for Pb^{206} agrees well with the shape of the corresponding theoretical curves of Jackson. However, unpredicted by this theory, the (p,2n) and (p,4n) cross sections peak relatively higher than the (p,3n) and (p,5n) curves. Accordingly the curve representing the sum of the measured (p,xn) cross sections occurring at each energy fluctuates sharply with main peaks occurring at about the same energies as the peaks of the (p,2n) and (p,4n) cross sections. Up to about 40 mev the experimental sum curve, averaged over fluctuations, follows $\sigma_c(p)$ for R about midway between 7.7 and 8.9 x 10^{-13} cm, corresponding to r_o = 1.3 and 1.5 x 10^{-13} cm respectively. Thus, an "average" R of about 8.3 x 10^{-13} cm is indicated for Pb^{206}; this gives r_o = 1.4 x 10^{-13} cm. The nuclear radius of natural lead has previously been derived from measurements of the total neutron cross section. As in the present work, the values obtained depend upon the model used to describe the reactions. Assuming that $\sigma_t = 2\pi R^2$, nuclear radii for natural lead of 8.40 and 8.49 x 10^{-13} cm were obtained for incident neutrons of energy 42 and 90 mev respectively[36,37]. Heckrotte[38] analysed the data for total neutron cross sections at 90 mev assuming a parabolic rather than a square potential well shape and using the optical model of Fernbach, Serber and Taylor[39]. A nuclear radius of 9.3 x 10^{-13} cm in place of 8.49 x 10^{-13} cm is obtained. According to the Fernbach-Serber-Taylor optical model

and assuming a square potential well the measured total neutron cross section for 95 mev neutrons indicates a nuclear radius for natural lead of 8.14×10^{-13} cm[40].

Above about 40 mev the experimental curve for the sum of the (p,xn) cross sections falls progressively lower than the $\sigma_c(p)$ curve. This is at least partly due to the increasing probability for the occurrence of reactions other than (p,xn). The general shape of the calculated $\Sigma \sigma_n$ curve of Jackson (Fig. 2) agrees qualitatively with the averaged experimental sum curve. (The calculated results were obtained using $r_o = 1.5 \times 10^{-13}$ cm. Therefore the cross sections are on the average higher than the experimental results for Pb^{206}.)

The magnitude of the high energy tail-off relative to the peak value of a (p,xn) curve seems somewhat higher for the measured lead cross sections than for the calculated curves of Jackson. Only the (p,2n) tail-off has been measured over an extensive energy range. It shows the same slowly changing shape as the theoretical curve but is about 50% higher relative to the peak.

Thresholds for the (p,xn) reactions in Pb^{206} occur at energies about two or three mev higher than thresholds for corresponding reactions in Bi^{209}. This can be ascribed to binding energy differences. The binding energy of the incoming proton is nearly two mev less in the case of Pb^{206} than for Bi^{209}. In addition, neutron binding energies appear somewhat greater in the bismuth nuclei involved in (p,xn) reactions in Pb^{206} than in the polonium nuclei involved in Bi^{209} (p,xn) reactions.

As was noted above, the measured even-xn cross sections peak relatively high with respect to the odd-xn cross sections in Pb^{206}.

While the (p,4n) curve, as determined, includes a small contribution due to the (p,p3n) reaction, this contribution is only appreciable beyond the peak where there is sufficient energy for this reaction to take place (through the prompt emission of one proton followed by three prompt and/or evaporation neutrons). The same argument holds for the (p,6n) curve. Internal cascade processes giving (p,p5n) and (p,2p4n) reactions are not important in the first portion of the curve.

There is, therefore, a striking similarity between the experimental results on Bi^{209} and those for Pb^{206}. In both cases emission of an even number of neutrons leads to a residual nucleus which is even in neutrons, although the number of protons is respectively even and odd. If the neutron binding energy were consistently higher in even-neutron nuclei in this mass region, the even-xn cross sections should be high. Higher thresholds for the odd-xn reactions would result in relatively more processes leading to states in even-neutron nuclei with insufficient energy for the emission of the next odd neutron. However, if this effect were great enough to cause the observed differences in cross sections the energy difference between the observed threshold for an even-xn reaction and the threshold for the next (odd)-xn reaction should be relatively greater than the energy difference between the threshold for an odd-xn reaction and the next even-xn reaction. This does not seem to be the case. In addition, one should not expect fluctuations in the sum curve. The even cross sections should simply be high at the expense of the odd ones.

A possible alternative explanation may account for the unexpected results. The present situation resembles in some ways that found with neutrons at relatively low energies. When averaged over resonances, the

total cross section for incident neutrons of energy up to about 14 mev shows broad fluctuations when plotted against the neutron energy or the mass number of the target nucleus[19][41]. The nature of these fluctuations changes only slowly with mass number. Slowly varying fluctuations in the average neutron cross section are not predicted by the Feshbach-Weisskopf theory[42] of nuclear reactions based upon the "strong-coupling model", although this theory explains the detailed behaviour, at least as to order of magnitude.

The fluctuations in the total neutron cross section do not seem to depend on detailed features of nuclear structure; but on some general properties which vary slowly with A, say the nuclear radius. Feshbach, Porter and Weisskopf[19] have used a model which explains the observed average total neutron cross section very well in the energy region from zero up to a few mev. A "gross-structure" problem is defined by appropriately averaging over resonances. The simple model consists in replacing the nucleus by a one-body potential which acts upon the incident nucleon. (The success of the shell model at low excitation energies indicates that a nucleon can move freely within the nucleus in a potential due to the other nucleons). This potential is complex; the real part represents the average potential in the nucleus; the imaginary part gives an absorption which describes the formation of the compound nucleus.

The main fluctuations in the total (p,xn) cross section curve for bismuth and lead resemble those for the average total neutron cross sections, although they occur at higher energies and are broader. In bismuth the two main peaks occur at about 18 and 40 mev while for lead they are found at about 23 and 45 mev. If they do in fact represent

fluctuations in the total reaction cross section, the peaks at about 23 and 45 mev would make the (p,2n) and (p,4n) cross sections peak relatively higher and the (p,3n) and (p,5n) cross sections relatively lower than expected from the theory which assumes a smoothly increasing capture cross section with increasing bombardment energy. The fact that the curve for the sum of (p,4n) and (p,p3n) cross sections in Pb^{206} is still relatively high at the energy of the (p,5n) peak may be partly due to the increasing importance of the (p,p3n) contribution at higher energies.

A study of (p,xn) cross sections in Pb^{207} should help greatly to resolve the origin of the unexpected results of the (p,xn) cross section measurements for bismuth and Pb^{206}. If the (p,2n) and (p,4n) cross sections were again found to be relatively high and the (p,3n) and (p,5n) cross sections relatively low it would be possible to discount the explanation in terms of a difference in the binding energy for a neutron in an odd- or even-neutron nucleus. For Pb^{207},(p,xn) reactions involving the emission of an even number of neutrons lead to nuclei with an odd number of neutrons and so should be relatively smaller according to this explanation. In addition, (p,3n) and (p,5n) reactions in Pb^{207} lead to the same radioactive products as (p,2n) and (p,4n) reactions in Pb^{206}; if the even-neutron cross sections in Pb^{207} were also high it would therefore be strongly evident that the irregularities in both Pb^{206} and Pb^{207} were not due to indeterminate and poorly known factors pertaining to particular radioactive decays. Lead samples enriched respectively in isotopes 207 and 208 are being acquired and further work is planned.

APPENDIX I

Sample Cross Section Calculation

These calculations are for the (p,3n) cross section in Pb^{206} at a proton bombardment energy of 27.8 mev. At this energy Pb^{206} is the only isotope contributing to the formation of Bi^{204}, the reaction product of Pb^{206} (p,3n) Bi^{204}. The decay proceeds as follows:

$$Bi^{204} \xrightarrow[12\ hr]{E.C.} Pb^{204m} \xrightarrow[1.1\ hr]{} Pb^{204}$$

A gamma ray of energy .374 mev is emitted in the decay of Pb^{204m} and was used to determine relative yields of the (p,3n) reaction at various bombardment energies. At a time after irradiation long enough so that the Pb^{204m} state is in equilibrium with the parent Bi^{204}, the decay of the .374 mev gamma ray shows the same half-life,- namely, 12 hr. The gamma ray activity at this bombardment energy corresponded to an initial K x-ray activity of

A_i = 2020 c/sec (distance from source to crystal = 10 cm.)

Also $n = 2.44 \times 10^{20}$ atoms/cm^2 of Pb^{206}

$p = 7.38 \times 10^{13}$ protons (from C^{11} activity in teflon)

$\lambda = 1.60 \times 10^{-5}$ sec^{-1}

The number c is determined from the following factors

(1) K- to total-electron capture ratio = 1/1.33

(2) Number of K x-rays per Bi^{204} decay due to internal conversion of gamma transitions is .27 + .10 = .37

(3) Fluorescent yield is 0.95

(4) Efficiency of counter for K x-rays at d = 10 cm is .0087

(5) Self-Absorption of K x-rays in source is 7%.

Thus, $C = 1.33 \times \frac{1}{1.37} \times \frac{1}{.95} \times \frac{1}{.0087} \times \frac{1}{0.93} = 126$

and, from equation 2.4 we obtain for the cross section,

$$\sigma = \frac{126 \times 2020}{1.60 \times 10^{-5} \times 2.44 \times 10^{20} \times 7.38 \times 10^{13}} = .88 \times 10^{-24} \text{ cm}^2/\text{atom of } Pb^{206}$$

APPENDIX II

Beam Current Integrator Circuit

The circuit diagrams for the power supply and integrator (built into the same chassis) are shown in Fig. 15.

Power Supply:

The 110v. feeding the primary of the transformer is stepped up to 480v by connecting two windings, of 240v each, in series in the secondary. Half wave rectification is followed by a π-filter consisting of a condenser, choke and condenser. With a 2K dropping resistor the VR chain draws up to 25 m.a. (for no load). Grounding of the centre point of the VR chain gives measured output d.c. voltages of +216v and -216v. The integrator circuit draws $\sim$6 m.a. between +216v and -216v and $\sim$5 m.a. between +216 and ground, so that the working current in the VR's is comfortably within their range.

The secondary windings of the transformer supply heater voltages of 5v for the rectifier tube and 6.3v for the integrator circuit.

Integrator Circuit:

This is essentially a modification of the circuit designed by Dr. R.E. Bell, and built into each channel of the McGill kicksorter. It is modified so as to integrate positive current and can be used to measure total integrated charge or instantaneous current.

The input positive current is smoothed out, if it is in pulse form, by the 1000 $\mu\mu$f condenser. It passes on to the integrating condensers or through the high value precision resistors depending on whether it is to be integrated or read off as an instantaneous current. The choice of function and range is made through the six-position non-shorting switch

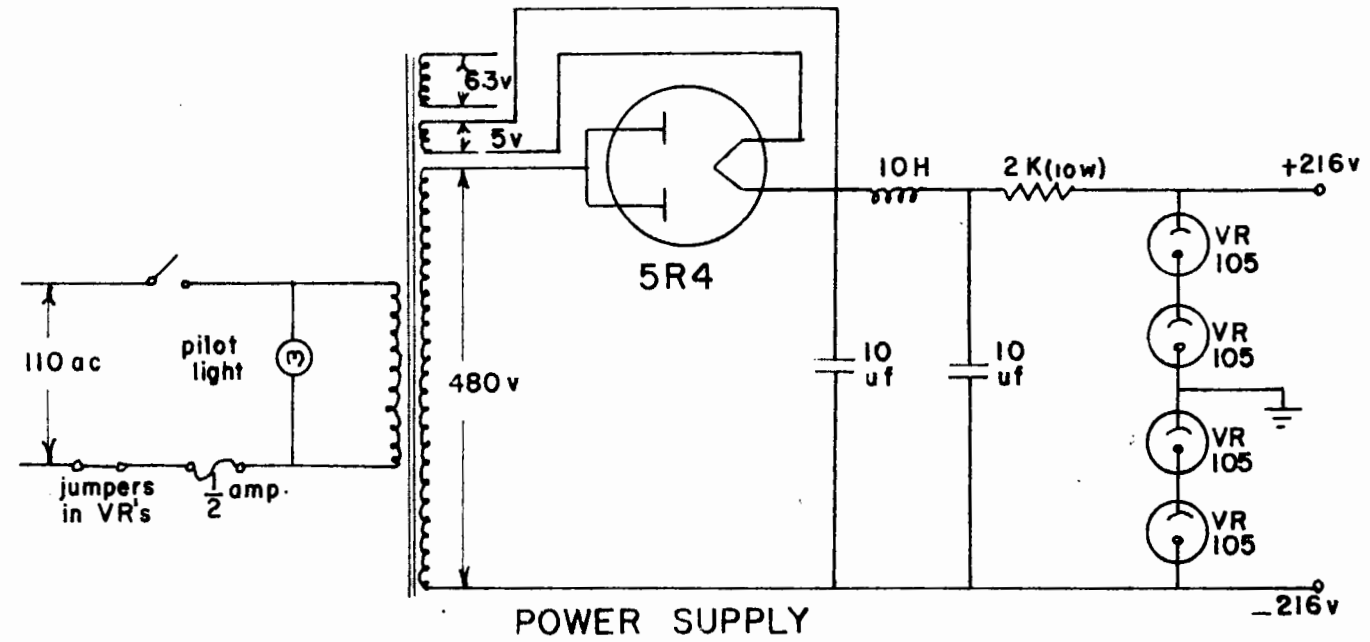

POWER SUPPLY

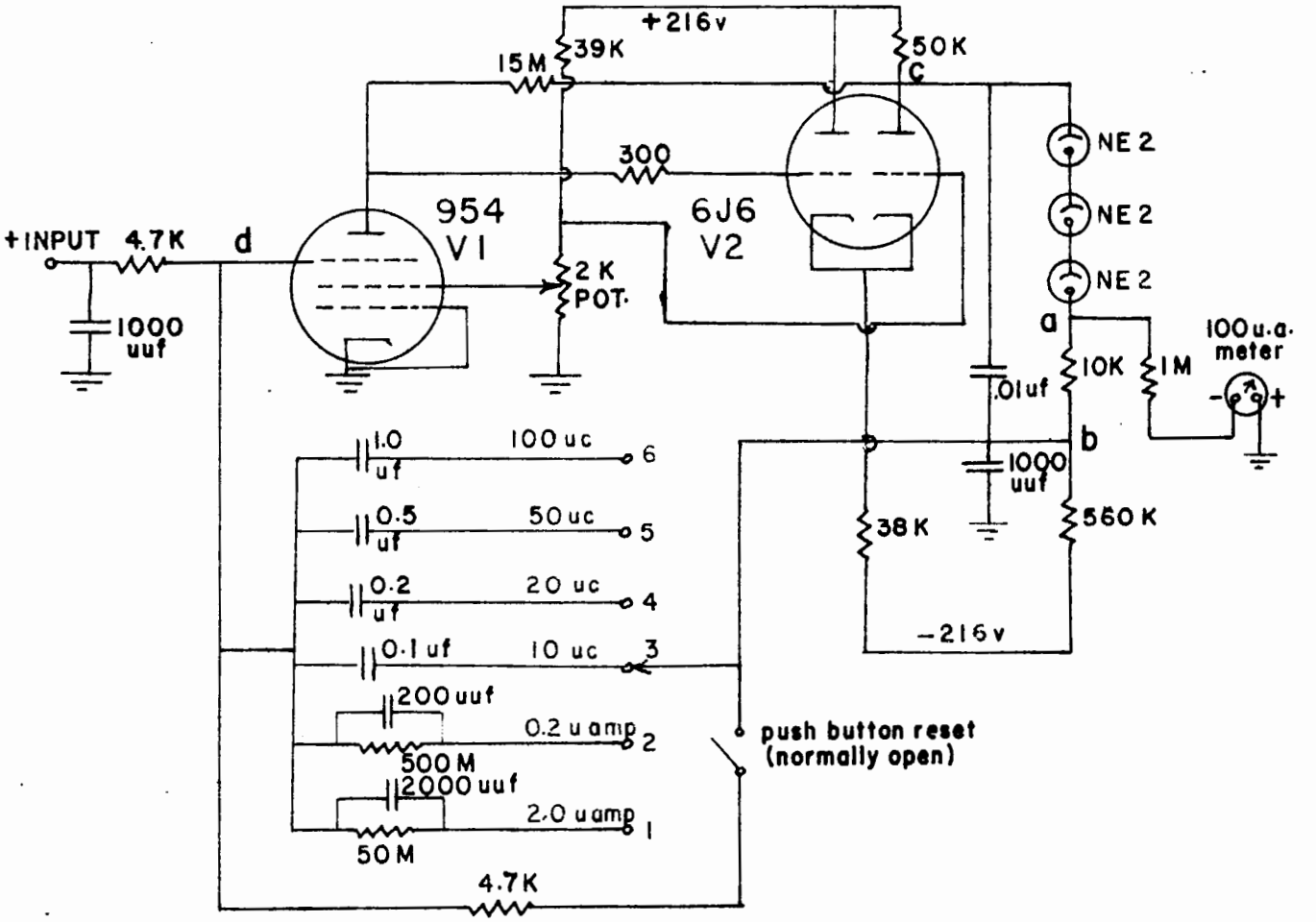

INTEGRATOR CIRCUIT

FIG. 15. PROTON BEAM CURRENT INTEGRATOR

shown. In any case, a voltage is produced across d-b. V1 and V2 comprise an amplifier of gain -175 which accepts the integrated or instantaneously monitored current. Thus, from the point of view of the voltage developed at d, the current "sees" an impedance which is 1/175 that of the particular integrating condenser or resistor through which it passes; if the voltage across d-b is 100v, the voltage at d has moved only about half a volt. This high gain is achieved partly through positive feedback. At the zero position with the push button switch closed, d + b assume a potential of about -4v. With this bias on V1 the right side of V2 draws a current which gives a voltage of about +165v at c. This voltage is dropped through three neon bulbs to give a zero output voltage at a. Zeroing is achieved through adjustment of the 2K potentiometer which controls the potential of the screen of V1. As the potential at d rises due to the incoming current, V1 turns on current and part of the current in the 6J6 is switched from the left half to the right half causing the potential at c (and at a) to fall. A meter connected to a as shown gives a full scale deflection of 100v. As indicated on the figure, this corresponds to total integrated charge or instantaneous current depending on the position of the functional switch. Use of the electrometer tube V1 as shown - and with its filament held at +10v - limits satisfactorily the grid (suppressor actually) current. The condensers and high value precision resistors used in the monitoring of the current are accurate to within 1%.

BIBLIOGRAPHY

(1) J.M. Blatt and V.F. Weisskopf 'Theoretical Nuclear Physics', p. 365-379, J. Wiley and Sons, New York.

(2) Ref. 1, p. 352-353

(3) M.M. Shapiro, Phys. Rev. 90, 171 (1953)

(4) R. Serber, Phys. Rev. 72, 1114 (1947)

(5) J.D. Jackson, Phys. Rev. 95, 651 (1954) and private communication

(5a) H. McManus, W.T. Sharp and H. Gellman, Phys. Rev. 93, 924(A) (1954) and private communication to J.D. Jackson

(6) H.L. Bradt and D.J. Tendam, Phys. Rev. 72, 1117 (1947)

(7) E. Bleuler, A.K. Stebbins and D.J. Tendam, Phys. Rev. 90, 460 (1953)

(8) S.N. Ghoshal, Phys. Rev. 80, 939 (1950)

(9) J.W. Meadows, Phys. Rev. 91, 885 (1953)

(10) E.L. Kelly - Ph.D. Thesis, University of California

(11) G.G. Andre et al (private communication)

(12) R.E. Bell, Phys. Rev. 95, 651 (1954), and private communication

(13) T.H. Handley and E. Newman, Phys. Rev. 95, 639(L) (1954)

(14) R.W. Fink and E.O. Wiig, Phys. Rev. 96, 185 (1954)

(15) A. Tomasini, Nuovo Cimento 12, 134 (1954)

(16) L. Rosen and L. Stewart (Los Alamos report No. 1560)

(17) E.B. Paul and R.L. Clarke, Can. J. Phys. 31, 267 (1953)

(18) J.S. Kirkaldy - Thesis, McGill University

(19) H. Feshbach, C.E. Porter and V.F. Weisskopf, Phys. Rev. 96, 448 (1954)

(20) R.L. Aamodt, V. Peterson, R. Phillips, UCRL - 1400 (1951)

(20a) N.M. Hintz, Bull. A.P.S. 26, 17 (1951)

(20b) W.E. Crandall, G.P. Millburn, R.V. Pyle, W.B. Birnbaum, UCRL-2756 (1955)

(21)W.H. Jordan and P.R. Bell, Rev. Sci. Inst. 18, 703 (1947)

(22) R.E. Bell - unpublished

(23) R.E. Bell - unpublished

(24) R.E. Bell and H.M. Skarsgard, Can. J. Phys. (To be published)

(25) The McGill Kicksorter, McGill Rad. Lab report by H.M. Skarsgard

(26) P.R. Bell, 'Beta- and Gamma-Ray Spectroscopy', Kai Siegbahn (Editor) North-Holland Publishing Co. (1955), pp 133-164

(27) F.K. McGowan, Phys. Rev. 93, 163 (1954) and private communication

(28) H. Brysk and M.E. Rose, ORNL 1830 (1955)

(29) I. Bergstrom, 'Beta- and Gamma-Ray Spectroscopy', Kai Siegbahn (Editor) North-Holland Publishing Co. (1955), p. 630

(30) J.M. Hollander, I. Perlman and G.T. Seaborg, 'Tables of Isotopes' reprint from Rev. Mod. Phys. 25, 469 (1953)

(31) D.E. Alburger and M.H.L. Pryce, Phys. Rev. 95, 1482, (1954)

(32) B.B. Kinsey, Can. J. Research A, 26, 404 (1948)

(33) I. Bergstrom and A.H. Wapstra, Phil. Mag. 46, 61, 1955

(34) A.H. Wapstra, D. Maeder, G.J. Nijgh and L. Th. M. Ornstein, Physica 20, 169 (1954)

(35) K.E. Bergkvist et al, Phil. Mag. 46, 65 (1955)

(36) R.H. Hildebrand and C.E. Leith, Phys. Rev. 80, 842 (1950)

(37) L.J. Cook et al, Phys. Rev. 75, 7 (1949)

(38) W. Heckrotte, Phys. Rev. 95, 1279 (1954)

(39) S. Fernbach, R. Serber and T.B. Taylor, Phys. Rev. 75, 1352 (1949)

(40) J. DeJuren and N. Knable, Phys. Rev. 77, 606 (1950)

(41) E.R. Graves and R.W. Davis, Phys. Rev. 97, 1205 (1955)

(42) J.M. Blatt and V.F. Weisskopf 'Theoretical Nuclear Physics', p. 311, J. Wiley and Sons, New York.